GEOCHEMICAL AND SEDIMENTARY RECORD OF URBANIZATION AND INDUSTRIALIZATION OF THE GALVESTON BAY WATERSHED

A Dissertation

by

MOHAMMAD E A Y S ALMUKAIMI

Submitted to the Office of Graduate and Professional Studies of
Texas A&M University
in partial fulfillment of the requirements for the degree of

DOCTOR OF PHILOSOPHY

Chair of Committee,	Timothy Dellapenna
Committee Members,	Peter Santschi
	Karl Kaiser
	Wesley Highfield
Head of Department,	Debbie Thomas

May 2016

Major Subject: Oceanography

ABSTRACT

Over the last 100 years, the Galveston Bay (GB) Estuary has experienced a wide range of anthropogenic activities. The bay's watershed and shoreline contains one of the largest concentrations of petroleum and chemical industries in the world, with the greatest concentration within the lower San Jacinto River/Houston Ship Channel (SJR/HSC). Extensive groundwater has been withdrawn to support these industries, and an expanding population has resulted in elevated land subsidence, with the highest rates in the lower SJR/HSC (3 cm yr^{-1}, > 3 m) decreasing seaward throughout the bay to 0.6 cm yr^{-1} near Galveston Island. Due to the industrial, commercial, and residential importance of the GB watershed, understanding the sources of sediment, and the rates of accumulation is imperative in determining the concentration, inventory and fluxes of trace metals (e.g., Hg) in the environment. Moreover, these data may be used to minimize the impact on public health, and reconstruct the historical input for improving management strategies. To examine the anthropogenic alteration in the system, 22 sediment vibra-cores were collected throughout the bay and analyzed using ^{210}Pb and ^{137}Cs radioisotope geochronology, grain size, XRF, X-radiography, Hg concentration, lignin content and composition, and stable carbon and nitrogen isotopes. Geochronology from these cores was used to determine sedimentation rates and correlated to Hg profiles to estimate input histories. The results show the highest sedimentation rates correspond to areas of highest Relative Sea Level Rise (RSLR), and are of the same order of

magnitude. In general, sedimentation rates are as much as 50% of RSLR, indicating that sedimentation has not kept pace with land subsidence. Profiles show significant input of Hg beginning in the 1900s, with highest concentrations between the 1960s-1970s, with a substantial decrease in concentration since, demonstrating it to be a valuable geochronology tool. Hg concentrations were found to be significantly higher proximal to the SJR/HSC, progressively decreasing seaward and to distal parts of the bay. Results of $\delta^{13}C$ and lignin analyses indicate there is a significant terrestrial input of organic matter, and the system has shifted from being a marine to terrestrial dominated system.

ACKNOWLEDGEMENTS

I would like to thank my committee chair, Dr. Timothy Dellapenna, and my committee members, Prof. Peter Santschi, Dr. Karl Kaiser, and Dr. Wesley Highfield, for their guidance and support throughout the course of this research. Special thanks to Dr. Patrick Louchouarn for allowing me to use his lab for my lignin analyses and providing me with extensive information and support. I would also like to thank Dr. Bob Presley and Dr. Gary Gill for their support and the valid advice, especially on mercury. Moreover, I would like to thank Dr. Anis and his wife Ruthy for providing me with love and Humus.

I am also grateful to the Texas Sea Grant and the Geological Society of America (GSA) for providing some of the necessary funding for this project. Publication supported in part by an Institutional Grant (NA14AR4170102) to the Texas Sea Grant College Program from the National Sea Grant Office.

Thanks also go to my friends (Allison Myers, Matt Norwood, and Kendra Kopp) and colleagues, and the department faculty and staff for making my time at Texas A&M University a great experience. I also want to extend my gratitude to past and present members the Coastal Geology Laboratory (especially Dr. Joshua Williams) and numerous other TAMUG graduate students for providing invaluable contributions to field and laboratory work. Thanks to my Kuwaiti friends and brothers, Dr. Fahad Al

Senafi and Tariq Al Rushaid for taking care of me and providing me with good company through out these five years.

This thesis is dedicated my mother and father for their encouragement and to my lovely and wonderful wife (Fatmah) and kids (Aisha, Ebrahim and Abdullah) for their patience, love, encouragement, and support provided. Living in the United States of America was life changing for me, and I will not ever forget it. Thank you USA, TAMU and Dr. Timothy Dellapenna for providing this opportunity to be part of the scientific community, and ultimately in becoming a better person.

NOMENCLATURE

^{13}C	Stable Carbon isotope	
^{14}C	Radioactive Carbon Isotope	
^{137}Cs	Radioactive Cesium Isotope	
^{15}N	Stable Nitrogen isotope	
^{206}Pb	Stable Lead isotope	
^{207}Pb	Stable Lead isotope	
^{210}Pb	Radioactive Lead Isotope	
$^{210}Pb_{total}$	Total ^{210}Pb Activity	dpm g^{-1}
$^{210}Pb_{xs}$	Excess ^{210}Pb Activity	dpm g^{-1}
^{209}Po	Radioactive Polonium Isotope	
^{210}Po	Radioactive Polonium Isotope	
A_0	Initial Activity	dpm g^{-1}
AD	Accretionary difference	
Ag	Silver	
Al	Aluminum	
Ar	Aragon	
A_z	Activity at depth	dpm g^{-1}
Bkg-Hg	Background Mercury Concentration	ng g^{-1}
CRM	Certified Reference Materials	
Cu	Copper	

d	Thickness of sediment	cm
E.F	Enrichment Factor	dimensionless
EPA	Environmental Protection Agency	
ESLR	Eustatic Sea Level Rise	cm yr^{-1}
GB	Galveston Bay	
GBNEP	Galveston Bay National Estuary Program	
GOM	Gulf of Mexico	
GPS	Global Positioning System	
GSLR	Global Sea Level Rise	
HCl	Hydrochloric Acid	
HF	Hydrofluoric Acid	
Hg	Mercury	
Hg flux	Mercury Flux	ng m^{-2} yr^{-1}
Hg Inv	Mercury inventory	ng m^{-2}
Hg Inventory	Mercury Inventory	ng m^{-2}
HGSD	Houston Galveston Land subsidence District	
HNO_3	Nitric Acid	
HPGe	High Purity Germanium	
HSC	Houston Ship Channel	
HSR	High Subsidence Regions	
I_{geo}	Geoaccumulation index	dimensionless
IPCC	Intergovernmental Panel on Climate Change	

ISR	Intermediate Subsidence Regions	
LOP	Lignin-derived Oxidation Products	
LSR	Low Subsidence Regions	
Max-Hg	Maximum Mercury Concentration	$ng\ g^{-1}$
Max-Hg depth	Depth of Maximum Mercury Concentration	$ng\ g^{-1}$
n	Number of Samples	
N_2	Atmospheric Nitrogen	
NaOH	Sodium Hydroxide	
NASA	National Aeronautics and Space Administration	
Ni	Nickel	
NOAA	National Oceanographic and Atmospheric	
Pb	Lead	
R^2	Coefficient of Determination	
RRF	Relative Response Factor	
RSD	Relative Standard Deviation	%
RSLR	Relative Sea Level Rise	$cm\ yr^{-1}$
S	Sediment Accumulation Rate	$cm\ yr^{-1}$
S-Hg	Surface Mercury Concentration	$ng\ g^{-1}$
S_{Avg}	Average sediment accumulation rate	$cm\ yr^{-1}$
SJR	San Jacinto River	
SRM	Standard Reference Material	
T-Hg	Total Dry Mercury	$ng\ g^{-1}$

$t_{1/2}$	Half Life	year
TCEQ	Texas Commission on Environmental Quality	
TEL	Tetraethyl lead	
TOC	Total Organic Carbon	%
TOM	Terrigenous Organic Matter	%
USACE	US Army Corps of Engineers	
USGS	United State Geological Survey	
VPDB	Vienna Pee Dee belemnite	
XRF	X-Ray Fluorescence	
ρ	Sediment Density	g cm^{-3}
α	Alpha Radiation	
Δ	Relative Change in Variable	
δ	Standard Reporting Delta Notation	
λ	Decay constant of ^{210}Pb (0.031).	$year^{-1}$
σ	Standard Deviation	
φ	Porosity	dimensionless

TABLE OF CONTENTS

LIST OF FIGURE

LIST OF TABLES

CHAPTER I

INTRODUCTION AND SYNOPSES

1.1 Introduction

The dissertation herein describes research conducted in the Galveston Bay watershed, located in the northern Gulf of Mexico, and investigates the impact of anthropogenic activities throughout the last century. With the fourth largest city and one-third of the of the US petroleum refining capacity located along its shores (Santschi et al., 2001), understanding sediment transport and geomorphology of Galveston Bay is relevant to both the public and private sectors. This investigation strives to increase our knowledge of the impact of anthropogenic alterations on the aquatic system, and evaluate the natural responses to these activities.

Galveston Bay is an ideal site to investigate the ability for an estuary to keep pace with rapid sea level rise and subsidence, as well as the implications in terms of the fate and transport of particle bound contaminants. Groundwater withdrawal has caused significant subsidence throughout the last century, which has increased the frequency and intensity of flooding, and damaging of the industrial infrastructure (Coplin and Galloway, 1999). With eustatic sea level projected to rise 1 m or more in the next century (IPCC, 2013), understanding the response estuaries will have is imperative. In the past century, subsidence in the upper GB caused relative sea level rise at three times this rate. The majority of studies within GB have focused on the effect of subsidence on

wetlands over the last 100 years. However, no studies have aimed to determine whether sedimentation within the bay kept pace with subsidence and the resultant increase in accommodation space. Furthermore, whether sedimentation could potentially keep pace with the projected elevated rise in sea level predicted for the near future. This research investigates whether sedimentation was able to keep pace with subsidence for the last 100 years in numerous depositional environments throughout GB. Since the highest rates of subsidence coincided with the period of highest inputs of mercury, this research was able to address the effectiveness of GB to either store or flush mercury under varying sedimentation regimes, furthering our understanding of the fate and transport of mercury. In addition, the utility of mercury as a geochronological tool was evaluated as a pseudo-independent dating technique.

Thus, the objectives of this study are to 1) address the response of sedimentation rates to subsidence throughout the last century, 2) determine if depositional environments have changed as natural response to anthropogenic alterations, 3) determine the concentration of mercury in marine sediments, and 4) assess Hg as a local/regional geochronological tool. These objectives were investigated utilizing ^{210}Pb and ^{137}Cs radioisotope geochronology, grain size analyses, X-ray fluorescence, X-radiography, mercury concentration, TOC, stable C and N isotopes, and lignin concentrations. The following sections represent an overview of each chapter.

1.2 Synopses of chapters

1.2.1 Sediment accumulation rate and land subsidence

Galveston Bay (GB) is the second largest estuary in the Gulf of Mexico, with the watershed containing one of the largest concentrations of petroleum and chemical industries globally, particularly within the lower 15 km of the San Jacinto River/Houston Ship Channel (SJR/HSC). Throughout the last century, extensive groundwater extraction to support these industries and an expanding population has resulted in significantly enhanced land subsidence (0.6-3.0 cm yr^{-1}). More distal areas in East and West Bays have subsidence rates on the order of 0.2 cm yr^{-1}, comparable to eustatic rates. In order to examine the impact of these anthropogenic alterations to the system, 22 vibracores were collected throughout the bay and ^{210}Pb and ^{137}Cs radioisotope geochronologies and grain size distributions were determined. Historical data documenting land subsidence rates for the last century revealed three distinctive regions along the shore of GB with elevated anthropogenically driven subsidence, which are areas with low, medium and high subsidence, respectively. Sediment accumulation rates show a gradient with the highest rates in SJR/HSC, and decreasing both seaward (along salinity gradient) and towards low subsidence regions. Average sediment accumulation rate ranges from less than 0.1 cm yr^{-1} in the distal portions of the bay to 1.9 ± 0.5 cm yr^{-1}, with highest rate proximal to Houston Ship Channel. These results indicate sedimentation rates are dramatically higher (1.4-1.9 cm yr^{-1}) in areas with elevated Relative Sea Level Rise (RSLR), and are on the same order as subsidence rates.

However, throughout most of GB sedimentation rates are lower (as much as 50%) than RSLR.

1.2.2 Historical input of contamination and biomarkers

The impacts of industrialization and urbanization throughout the last century in Galveston Bay has resulted in significant shifts in trace metals and biomarkers recorded within the sedimentary record. A total of 22 sediment cores were collected in the bay in order to reconstruct the historical input of Hg, trace metals and lignin. Total Hg concentration ranged between 6 - 162 ng g^{-1} in surface sediment, and show a decreasing gradient from the Houston Ship Channel (HSC) toward the open estuary. Core profiles of Hg and trace metals show significant input beginning around 1900, with peak concentrations in the 1960-70's, and decrease thereafter. This ubiquitous timing suggests the potential use of Hg and other contaminants as a geochronological tool. Stable isotopes and lignin phenols show there is a significant terrestrial input of organic matter, and the provenance has shifted from being marine to terrestrially dominated, driven by land development within the watershed. The enrichment factor and the geoaccumulation index (I_{geo}) have been calculated to assess the effectiveness of environmental management practices, and show significant improvements since the 1970s. The natural recovery rate in Galveston Bay since the peak input of trace metals was non-linear and displays a reduction in recovery time during the twenty-first century. These results show the difference between the influence of industrialization and urbanization on the Galveston Bay aquatic systems.

CHAPTER II

SEDIMENT ACCUMULATION RATE AND RELATIVE SEA LEVEL RISE IN GALVESTON BAY

2.1 Introduction

With the rapid increase in coastal population (IPCC, 2007) over the past century, many estuaries around the world have been subjected to major anthropogenic alterations, including loss of freshwater inflow due to riverine damming (Barusseau et al., 1998; Gao et al., 2012b; Williams, Lee, et al., 2015; Williams et al., 2013), extensive land use changes (Williams et al., 2014; Yoon et al., 2007), increased population growth (McGranahan et al., 2007), dredging and dredge spoil dumping (Mitchell and Uncles, 2013; Yeager et al., 2010), land reclamation (Healy and Hickey, 2002; McLusky et al., 1992; Wu et al., 2002) installation of tidal and estuarine dams (Williams et al., 2014; Williams, Lee, et al., 2015), as well as extensive growth in urbanization and industrialization (Williams et al., 2014; Santschi et al., 2001, Ravichandran, 1995). These modifications have caused serious environmental changes, including shoreline retreat, subsidence, wetland losses (Feagin et al., 2005; Kennish and Paerl, 2010), altered tidal prisms, and changes in sediment dynamics and increased sediment toxicity (Tonis et al., 2002; Williams et al., 2014). It is expected that anthropogenic impacts due to land-use alterations will escalate during the twenty-first century (Donnelly and Bertness, 2001).

Relative sea-level rise (RSLR), as a combined result of eustatic sea-level rise (ESLR) and local uplift/subsidence, is a critical process currently affecting sedimentary processes in estuaries around the world. ESLR is predicted by the Intergovernmental Panel on Climate Change (IPCC) to rise by 0.26-0.55 m by the end of the twenty-first century (IPCC, 2013). Additionally, in regions where there is a high rate of subsidence due to groundwater extraction, RSLR is often much greater than ESLR. Despite the current rate of ESLR of 0.19 (0.17 to 0.21) cm yr^{-1} (Church et al., 2013), RSLR in a number of coastal systems and riverine basin has been reported at an order of magnitude greater than ESLR. The predicted increase in ESLR and RSLR has led to concerns regarding the stability and the existence of estuaries (Kennish, 2002; Lambeck and Chappell, 2001; Wolanski and Chappell, 1996).

Table 2.1 RSLR and major causes in costal systems and riverine basin around the world. GW is ground water withdraw. CD is canal dredging. SD is sediment diversion. LR is land reclamation. HP is high population.

Location	RSLR ($cm\ yr^{-1}$)	Causes	References
Bangkok	10	GW	(Nutalaya et al., 1996)
Taiwan	9	GW	(Jelgersma, 1996)
Tokyo	8.3	GW	(Jelgersma, 1996)
Mississippi delta	1	GW, CD, SD	(Penland and Ramsey, 1990)
Nile delta	0.5	LR, HP, CD	(Stanley, 1988)
Chesapeake Bay	0.39	GW	Eggleston and Pope (2013)
Venice Lagoon	0.15	LR	(Carbognin et al., 2004)

As a highly urbanized estuary, Galveston Bay is an ideal site to investigate the ability for sedimentation rates to keep pace with rapid RSLR rates. Due to the development of hydrocarbon refineries, withdraw of subsurface fluid (water and oil) has caused significant subsidence and faulting, increasing the frequency and intensity of flooding as well as damaging the industrial infrastructure (Kolker et al., 2011; Lester

and Gonzalez, 2002). Anthropogenically enhanced subsidence rates throughout the bay have existed since approximately 1900, became accelerated in the early 1940's due to the WWII efforts, and peaked in the mid-1970s (Coplin and Galloway, 1999). The red contour lines in figure 2.1 show the interpreted subsidence data provided by the Houston-Galveston Area Subsidence District. It should be noted that all of their measuring stations, not shown here, were land-based. Interpretations of subsidence rates were projected across the bay from their land-based stations. Subsidence rates vary significantly spatially, with lower subsidence trending towards the south and within East and West Bays (Figure 2.1). Throughout the Galveston Bay area, accelerated subsidence has caused loss of habitat and salt marsh erosion during the last century (GBNEP, 1994; HGSD, 2013; Lester and Gonzalez, 2011; Ravens et al., 2009; USGS, 2002). In addition to the monitoring of subsidence within the mainland shoreline of Galveston Bay, the National Oceanographic and Atmospheric (NOAA) tidal station on Pier 21 on the bayside of Galveston Island has collected a continuous hourly water level time series since 1904 and has recorded an average RSLR rate of 0.65 cm yr^{-1} (NOAA, 2013). This rate has been widely applied as a regional rate (Ravens et al., 2009). However, it should be noted that Pier 21 sits over the +30 m deep Trinity River incised valley, discussed below, and has experienced differential compaction (Anderson, 2007). Consequently, subsidence rates within the Trinity River incised valley, including the Pier 21 Tidal Gauge rates, are going to be higher than those areas outside of the valley and rates calculated from within the valley likely do not reflect regional rates and should be used with caution.

Estuaries such as Galveston Bay, on geological time-scales, are commonly considered ephemeral, geomorphological features that exist during transgression (prolonged rising of sea level) where sediment fills the accommodation space created by RSLR (Anderson, 2011). If the sediment supply cannot keep pace with RSLR (deficit), the estuary will deepen and transgress landward. Conversely, if sedimentation rates exceed the rate of accommodation space creation (surplus), the estuary will fill and prograde into a delta (Nichols, 1989). Thus, for estuaries to be maintained, equilibrium must exist between sediment supply, accommodation space, and RSLR (Bianchi, 2007; Day et al., 2013)

The impact of sediment accumulation rate and RSLR on the Galveston Bay system has been previously investigated in numerous studies. White et al. (2002) determined that a sedimentation rate of 0.5 cm yr^{-1} in Trinity River bayhead delta was lower compared to RSLR of 1.1 cm yr^{-1}, leading to marsh erosion due to the increase in the water volume. Similar results were found by Yeager et al. (2007) in the lower Trinity River floodplain, where sediment accumulation rate of 0.16 cm yr^{-1} were 84% lower than the RSLR in this region. Furthermore, sediment accumulation rate in West Galveston Bay salt marshes were found to be lower (0.2 cm yr^{-1}) relative to RSLR (0.65 cm yr^{-1}) (Ravens et al., 2009). As a result, wetlands are unable to keep pace with RSLR, which has been attributed as the major cause of salt marsh erosion (Ravens et al., 2009). However, as noted above, the use of the 0.65 cm yr^{-1} RSLR by Ravens et al. (2009) is based off of the Pier 21 Tidal gauge and is likely a significant overestimate of the actual rates. Based on records of dredging and filling operations, Ward (1993) reported that

the volume of Galveston Bay increased over 9.9 x 10^6 m^3 since 1900. Using historical maps and isopach charts, Shepard (1953) reported long-term sediment accumulation rate of 0.35 cm yr^{-1} for the entire bay. Furthermore, Rehkemper (1969) reported a sedimentation rate for the entire bay of 0.38 cm yr^{-1} based on radiocarbon dates (C^{14}) from 30 borings.

Although these studies have provided insight into the sediment accumulation rate and RSLR, they lack the spatial resolution to assess impacts throughout the Galveston Bay system. Furthermore, the methodology utilized (C^{14}) is limited in scope to century to millennial time-scale sediment accumulation rate. The rapid land subsidence within the upper Galveston Bay has resulted in a RSLR up to +3 m in the last century, resulting in the creation of new accommodation space. This occurred concomitantly with a dramatic increase in population and petrochemical facilities within the watershed, particularly along the shoreline of the bay. Therefore, it is the objective of this study to address subsidence along with sedimentation rates obtained from short-lived radioisotopes in Galveston Bay to determine whether the depositional environment has changed as a natural response to anthropogenically enhanced subsidence.

2.2 Regional setting

The Galveston Bay watershed contains Houston, the fourth largest city and fifth largest metropolitan area in the United States, with a population of about five million people residing around Galveston Bay (EPA, 2007; Lester and Gonzalez, 2011). Additionally, the region immediately adjacent to the bay contains one-third of the United States petroleum refining capacity, along with associated chemical industries (Morse et al., 1993; Santschi et al., 2001). Located on the southeastern shore of the upper Texas Gulf Coast, Galveston Bay (Figure 2.1) is the second largest natural semi-enclosed subtropical estuarine system in the Gulf of Mexico (Santschi et al., 2001) and the seventh largest in the United States (Yeager et al., 2010). The bay covers a surface area of 1554 km^2 surrounded by 526 km^2 of marshland (Pinckney et al., 2002). Galveston Bay is classified as a coastal plain estuary, which formed due to the submergence of the incised Trinity and San Jacinto River Valleys. These valleys were incised during the last low stand in sea level and were 35-40 m deep (Rodriguez et al., 2005). Inundation was initiated approximately 9,000 yBP as Holocene sea levels rose, reaching the current configuration around 2,500 yBP (Rodriguez et al., 2005). These valleys are largely filled with unconsolidated bay head delta sands and estuarine muds. The valley was incised into hard, indurated Pleistocene terraces and paleosols primarily the Beaumont Formation (Blum et al., 2003; Rodriguez et al., 2005; Siringan and Anderson, 1993). As a result, due to differential compaction of the unconsolidated Holocene incised valley fill and the hard, indurated valley walls, there is likely a higher

RSLR rate from locations within the incised valley when compared with those areas outside of the incised valley.

The bay is composed of five major sub-bays: Upper Galveston Bay, Lower Galveston Bay, Trinity Bay, West and East Bays (Figure 2.1). Galveston Bay is a micro-tidal, turbid, wind-dominated estuary with an average water depth of 3 m (Wen, Santschi, et al., 1999) and primarily astronomical diurnal tides (Anderson, 2011). In addition, Clear Lake and Taylor Lake are minor sub-bays with an average water depth of 2 m (Figure 2.1). Fresh water input to Galveston Bay is primarily from the Trinity River (83%) and San Jacinto River (8%), with Chocolate Bayou as a minor source (Orlando et al., 1993) The major tidal inlet in this system is Bolivar Road, which is located between Galveston Island and Bolivar Peninsula (Figure 2.1). At the western end of Galveston Island, San Luis Pass is an additional major tidal inlet servicing the tidal prism of Christmas and West Galveston Bays. San Luis Pass separates Galveston Island from Follets Island. In addition, there is a small tidal cut located at Rollover Pass that services a portion of the East Galveston Bay tidal prism (Figure 2.1). Due to the presence of the extensive barrier islands, water exchange with the Gulf of Mexico is restricted, and the bay has an average water residence time of 40 days (Solis and Powell, 1999).

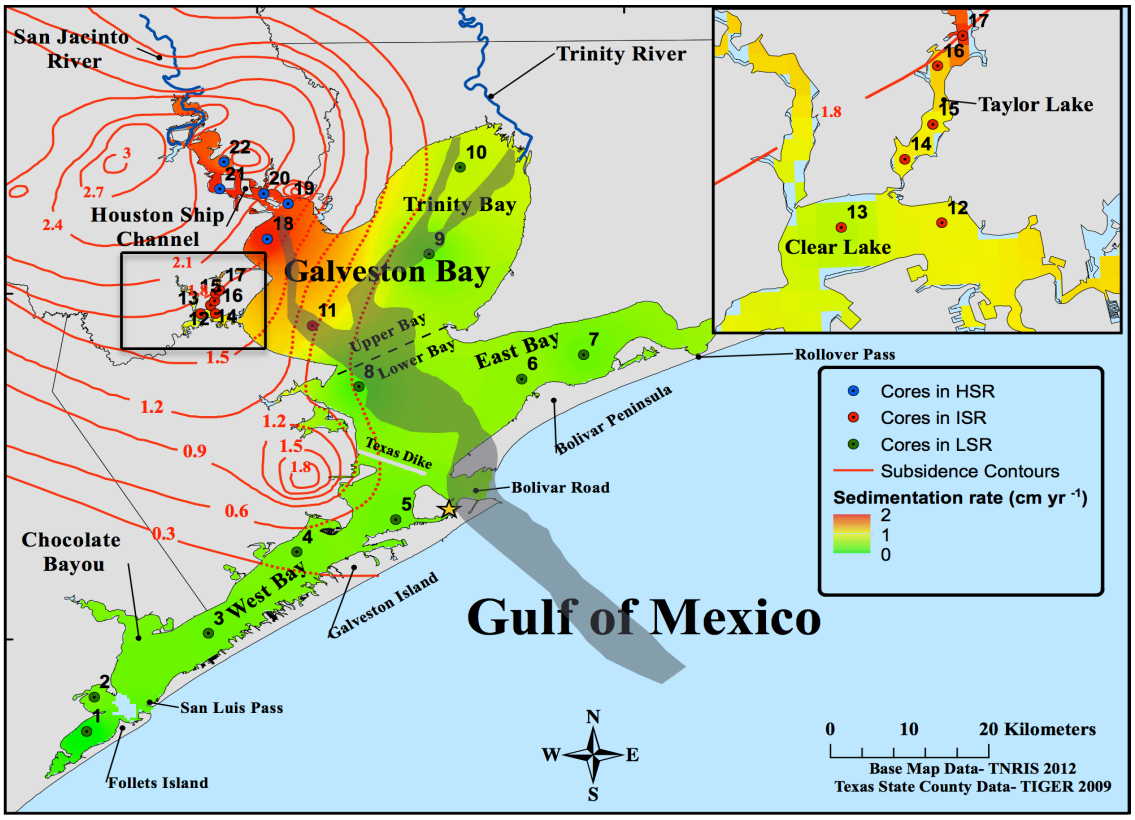

Figure 2.1 Detailed study area map showing all core sampling locations that have been characterized herein as Low Subsidence Regions (LSR), Intermediate Subsidence Regions (ISR), and High Subsidence Regions (HSR). Contour plot (red line) of subsidence (meters) between 1906 and 2000 (HGSD, 2008). Interpolated average sediment accumulation rate for the Galveston Bay Estuary. Data obtained from ^{210}Pb and ^{137}Cs geochronology from all core location. The yellow star indicates the location of the tidal gauge at pier 21(NOAA, 2013). The gray shaded area represents the Trinity River incised valley (Rodriguez et al., 2005).

2.3 Material and methods

2.3.1 Data collection and core processing

A total of 22 sediment vibracores (Figure 2.1) were collected from Galveston Bay on five cruises (June 15, July 27, August 1 and 8, 2012, and April 30, 2014) using 7.6 cm diameter aluminum core barrels, with recovery rates ranging from 1-3 m. Sample locations were chosen at sites where there is no known history of dredging. None of the Galveston Bay cores were collected over the thalweg of the incised Trinity River valley. Cores were sealed immediately and subsequently stored at 4°C for further processing and analyses. The recovered cores did not show any signs of degradation from transportation. Each core was cut in half lengthwise and digital photographs were taken at 20 cm interval and mosaicked. The core was sectioned at 1 cm intervals for the upper 10 cm, every 2 cm for 10 cm to 50 cm, and every 5 cm thereafter. The subsamples were homogenized, and stored in labeled Whirl-Pak bags until further processing.

2.3.2 Water content and porosity

Samples (10 g) from various depths in these cores were immediately placed in pre-weighed aluminum tins and kept in an oven at 50°C for at least 24 hours, and then re-weighed to determine water content. The porosity was calculated from the water content by estimating the salt content and the sediment density of 2.65 g cm^{-3}.

2.3.3 Grain size analyses

Wet sediment samples at 5 cm depth intervals from cores were analyzed in the laboratory for grain size distribution using Malvern Mastersizer 2000. A laser diffraction technique is used to determine the particle size by measuring the light scattered intensity from the dispersed particles in a liquid medium. About 2-4 g of the wet samples were homogenized and placed in a 100 mL glass jar. Ten milliliters (10 mL) of 5.5 g L^{-1} of sodium hexametaphosphate were added to the sediment samples as a dispersant solution and approximately 20 mL of deionized water was added to the jar. To disaggregate the samples, the jars were sonicated for 30 minutes at 25 $^{\circ}$C and frequency of 40 kHz. Because the Malvern instrument has a range of 0-2000 μm, all samples were wet sieved after sonication in a 2 mm sieve into 200 mL glass jar. The larger fraction of the samples, such as shells, were placed in pre-weighed aluminum tins and kept in an oven for at least 24 hours, and then re-weighed to determine the final grain size distribution. The jar with samples of < 2mm were filled with deionized water to a volume of 200 mL. The jars were placed on a stir plate to mix the samples. Ten milliliters (10 mL) from the stirring samples was pipetted into pre-weighed aluminum tins and dried in the oven for at least 24 hours, and then re-weighed for the weight percentage calculation. The stirring samples were pipetted into the instrument until the obscuration level was reached. Triplicate measurements of sand, silt, and clay fractions were made for each sample and the results were averaged. The results obtained from the Malvern in addition to the 10 ml sample that was removed, with the percentage of the fraction more than 2 mm were added to calculate the final percentage grain size composition.

2.3.4 Radioisotopes analyses

Short-lived radioisotopes have been used extensively to investigate sedimentary processes and accumulation rate in a variety of coastal and marine settings, including deltas, bays, estuaries, and continental shelves using time markers or using the profile of radiochemical with a known decay rate (Dellapenna et al., 1998; Nittrouer et al., 1984; Yeager et al., 2004)

The activity of ^{210} Pb ($t_{1/2}$ = 22.3 yr, Eγ= 46 KeV) was measured indirectly using its granddaughter ^{210} Po where they are assumed to be in secular equilibrium following the methods described by Nittrouer et al. (1979) and Santschi et al. (1999). Dry sediment samples at 5 cm intervals were pulverized, homogenized and wet sieved through a 38 μm sieve using deionized water. Then, approximately 1 g of the smaller fraction of each sample were placed in Teflon beakers and spiked with 0.25 μl of known activity of ^{209} Po tracer to assess the recovery of ^{210} Po. The samples were then digested with 15 ml of concentrated HCl and HNO_3, and 10 ml of HF. For some samples, HF was not used. The Teflon beakers were placed on hotplates to near dryness. After dryness, 15 ml of HCl and HNO_3, were added and the same procedure was repeated. Then, 15 ml of HCl was added and the Teflon beakers were baked to near dryness. Then, 50 ml of 1.5 N HCl was added to the sediment samples and ascorbic acid was added and stirred to the leachate to complex the free Fe (III). Silver planchets with one side exposed (1 cm^2) were placed to each leachate along with a magnetic stir bar. The solution was then stirred for about 12 hours and both ^{209} Po and ^{210} Po were electroplated onto the silver planchets. The silver planchets were removed and counted for 24 hours by α spectroscopy using a

CANBERRA surface barrier detector. The activity of ^{210}Pb was obtained from the counts ratio of the Po isotopes and the relative activity of the spiked sample. Excess ^{210}Pb ($^{210}Pb_{xs}$), was calculated as the difference between total activities and supported activities. The supported activity was determined from constant ^{210}Pb activities at depth. An average of 1 dpm g^{-1} was applied for cores not reaching the supported level. Average sediment accumulation rate were determined by calculating a logarithmic regression line using the following equation:

$$S_{Avg} = \frac{\lambda \Delta z}{\ln(A_0/A_z)}$$

Where S_{Avg} = Average sediment accumulation rate (cm y^{-1}), λ = decay constant of ^{210}Pb (0.031 $year^{-1}$), Δz = change in depth of the regression (cm), A_0 = $^{210}Pb_{xs}$ activity at beginning of regression (dpm g^{-1}), A_z = $^{210}Pb_{xs}$ activity at end of regression (dpm g^{-1})

The activity of ^{137} Cs ($t_{1/2}$ = 30 yr) was measured by gamma spectroscopy ($E\gamma$= 662 KeV) using a semi-planar intrinsic germanium detector coupled with Canberra DSA-1000 16K channel integrated multichannel analyzer using CANBERRA Genie 2000 spectroscopy software. Wet samples were homogenized and placed in 70 ml petri dishes, and counted for 2 days. Identical geometries were used for all samples. Two radioactive standards (NIST, SRM 4357 and Cs-137 standard FF-294, Isotopes Products Laboratories) were used on each detector to determine the efficiency factors at the required gamma ray energy. The net counts of each sample were converted to activity by using the efficiency factor and the wet weight of each sample. Sedimentation rate from ^{137} Cs was calculated from the depth of maximum activity, which occurs in 1963 from atmospheric atomic bomb testing (Santschi et al., 1999), and the time difference

between the peak and the data assayed (50 years for this study). Using these dating methods, the assumptions are made such that isotopes are scavenged by finer particles regardless the pathway that these isotopes enter the estuarine environment, and residence time of the water column is short compared to the half-life of the isotopes (Dellapenna et al., 1998; Santschi and Honeyman, 1989; Williams et al., 2014).

2.4 Results

2.4.1 Subsidence and relative sea-level rise

Examination of the subsidence data revealed 3 distinctive regions that have been characterized herein as Low Subsidence Regions (LSR), Intermediate Subsidence Regions (ISR), and High Subsidence Regions (HSR). Representative examples of these regions are shown in Figures 2.2, 2.3, and 2.4, respectively. LSR include West and East Bay, Texas City and Trinity Bay, where the subsidence was < 0.6 m between 1906-2000 (Figure 2.2). Based on the total subsidence reported for the last 94 years (HGSD, 2008), the average annual subsidence rate was calculated for each core location. The 10 cores collected within this region have been determined to have subsidence rates ranging from 0.19 cm yr^{-1} (Core 1) to 0.63 cm yr^{-1} (Core 8) (Table 2.2). Clear Lake, Taylor Lake, and Upper Galveston Bay are located in an ISR where there has been total subsidence between ≥ 0.6 m and ≤ 1.8 m. The 7 cores as an ISR represent a range in subsidence rate from 1.46 cm yr^{-1} (Core 11) to 1.91 cm yr^{-1} (core 17).

Table 2.2. Summary of grain size, sediment accumulation data derived from ^{210}Pb and ^{137}Cs geochronology and Relative Sea-Level Rise (RSLR) for Galveston Bay (GB). RSLR is the sum of subsidence rage in GB and the ESLR (0.19 cm yr^{-1}). Cores are separated by subsidence region (SR), low subsidence region (LSR), intermediate subsidence region (ISR), and high subsidence region (HSR) (locations shown in Figure 2.1) and core lengths are shown in cm. Sand, silt, and clay percentages represent average calculated from all samples within each core at a maximum sampling interval of 5 cm with errors shown as 1σ. An average of the two isotopes rate was calculated (S_{Avg}) and subsequently used for further correlation analyses. Accretionary difference (AD) is average accumulation rate minus RSLR. Note: accumulation rates could not be calculated for cores with no $^{210}Pb_{xs}$ activity or clear ^{137}Cs peak.

Region	Core	SR	Length (cm)	Avg. sand %	Avg. silt %	Avg. clay %	^{137}Cs S_{Avg} (cm yr^{-1})	^{210}Pb S_{Avg} (cm yr^{-1})	S_{Avg} (cm yr^{-1})	RSLR (cm yr^{-1})	AD (cm yr^{-1})
West Bay	1	LSR	136	26.0 ± 16.1	36.2 ± 3.70	37.8 ± 16.6	-	0.05 ± 0.01	0.05	0.38	-0.33
	2	LSR	171	31.5 ± 17.9	35.2 ± 6.50	31.1 ± 14.4	-	0.34 ± 0.09	0.34	0.38	-0.04
	3	LSR	176	38.1 ± 11.2	35.8 ± 9.10	24.2 ± 5.00	0.31	0.25 ± 0.04	0.28	0.68	-0.40
	4	LSR	242	33.7 ± 10.4	32.1 ± 7.10	28.9 ± 8.10	0.41	0.25 ± 0.04	0.33	0.68	-0.35
	5	LSR	241	53.0 ± 15.6	22.2 ± 9.50	22.3 ± 6.40	0.22	0.36 ± 0.20	0.29	0.71	-0.42
East Bay	6	LSR	201	35.4 ± 21.5	28.0 ± 12.1	24.9 ± 14.9	0.44	0.45 ± 0.06	0.44	0.68	-0.24
	7	LSR	232	18.4 ± 15.1	39.6 ± 12.5	35.2 ± 11.0	0.30	0.30 ± 0.05	0.30	0.68	-0.38
Texas City	8	LSR	97	38.9 ± 15.0	23.2 ± 7.70	23.0 ± 7.90	-	0.20 ± 0.05	0.20	0.82	-0.62
Trinity Bay	9	LSR	202	17.4 ± 10.0	44.3 ± 6.10	36.9 ± 10.3	0.30	0.27 ± 0.06	0.28	0.74	-0.46
	10	LSR	212	13.5 ± 10.5	46.0 ± 7.50	38.4 ± 11.3	0.58	0.60 ± 0.20	0.59	0.74	-0.15
Upper Bay	11	ISR	222	35.5 ± 11.3	39.3 ± 4.60	25.5 ± 8.30	-	-	-	1.65	-
Clear Lake	12	ISR	171	24.1 ± 9.30	53.0 ± 3.10	22.9 ± 9.40	-	1.00 ± 0.10	1.00	1.97	-0.97
	13	ISR	186	28.1 ± 15.8	50.6 ± 6.30	20.9 ± 10.3	1.34	1.00 ± 0.10	1.17	1.97	-0.80
Taylor Lake	14	ISR	225	26.9 ± 15.8	49.5 ± 8.70	22.7 ± 11.2	-	-	-	2.01	-
	15	ISR	241	22.6 ± 11.2	57.4 ± 6.10	20.0 ± 8.40	-	0.80 ± 0.10	0.80	2.04	-1.24
	16	ISR	221	20.4 ± 9.50	52.3 ± 6.50	27.3 ± 10.1	-	0.80 ± 0.10	0.90	2.07	-1.17
	17	ISR	216	26.7 ± 12.6	48.3 ± 6.60	25.0 ± 9.00	-	1.40 ± 0.30	1.40	2.10	-0.70
Houston Ship Channel	18	HSR	187	35.7 ± 8.90	46.4 ± 2.70	17.8 ± 7.20	-	1.50 ± 0.30	1.50	2.30	-0.80
	19	HSR	162	26.2 ± 24.8	41.6 ± 13.0	31.3 ± 14.0	-	-	-	2.46	-
	20	HSR	417	14.8 ± 12.9	56.9 ± 11.2	28.3 ± 12.7	-	1.40 ± 0.20	1.40	2.46	-1.06
	21	HSR	202	21.8 ± 16.6	42.0 ± 7.40	36.2 ± 11.4	-	1.90 ± 0.50	1.90	2.62	-0.72
	22	HSR	142	13.2 ± 24.1	42.7 ± 9.90	43.9 ± 15.7	1.5	1.5 ± 0.30	1.5	2.78	-1.28

The Houston Ship Channel is located in the region where the subsidence is high (HSR) ≥ 1.8 m, with the five cores collected in this region representing values ranging from 2.11 cm yr^{-1} (Core 18) to 2.59 cm yr^{-1} (Core 22). Historical subsidence values for each core obtained from HGSD (2008) and average ESLR (0.19 cm yr^{-1}) were summed to calculate the average relative sea-level rise rate throughout the last century, and have been summarized by subsidence region in Table 2.2.

2.4.2 $^{210}Pb/^{137}Cs$ geochronology

Profiles of $^{210}Pb_{xs}$ activity show variable excess activity throughout and more uniform near the surface suggesting a layer of intense sediment mixing. Examination of x-radiographs associated with each core found limited evidence of bioturbation, with most intervals containing preserved bedding which suggests mixing within the surface intervals of the cores was due to physical mixing rather than bioturbation and that decreases of radioisotope activities in core profiles result from sediment accumulation and decay rather than bioturbation. Representative profiles of $^{210}Pb_{xs}$ activity for the three distinctive subsidence regions are also shown in Figures 2.2, 2.3, and 2.4, respectively. On a decadal timescale, the sediment accumulation rate was assessed as valid based on sufficiently high R^2 values (>0.65) of the regression line. The $^{210}Pb_{xs}$ activity in cores collected in the LSR have been determined to have an averaged sedimentation rate of 0.31 ± 0.14 cm yr^{-1}, with rates ranging from 0.05 ± 0.01 cm yr^{-1} (Core 1) to 0.60 ± 0.20 cm yr^{-1} (Core 10). The $^{210}Pb_{xs}$ activity in the ISR displays a moderate average sediment accumulation rate of 1 ± 0.25 cm yr^{-1}, with values ranging

from 0.8 ± 0.10 cm yr^{-1} (Core 15) to 1.40 ± 0.30 cm yr^{-1} (Core 17). A higher average sediment accumulation rate (1.5 ± 0.22 cm yr^{-1}) was determined in the region of higher subsidence rate (HSR), with a range from 1.5 ± 0.30 cm yr^{-1} (Core 22) to 1.90 ± 0.50 cm yr^{-1} (Core 21). Core length, subsidence region and accumulation rate determined by ^{210}Pb and ^{137}Cs methods have been summarized and averaged in Table 2.2 (Error shows as 1σ). The maximum ^{137}Cs activity depths associated with the maximum fallout of the radionuclide in 1963 are shown in Figures 2.2, 2.3, and 2.4. The maximum ^{137}Cs activity was not determined in some cores because there was not a clear maximum peak.

2.4.3 Grain size profile

Profiles of grain size are shown as percent composition of shell, sand, silt, and clay (Figures 2.2, 2.3, and 2.4). The average relative grain size distribution for all cores is summarized in table 2.2. In general, each core has a vast range of grain size distribution with major variation between cores, which reflect the depositional environment. Considering average data from the 3 distinctive subsidence regions, the sediment composition of the Low Subsidence Region (LSR) has an average sand (30.6 ± 12.0%), silt (34.3 ± 8.1%), and clay (30.3 ± 6.4%) content. The Intermediate Subsidence Region (ISR) cores yield an average sand (26.3 ± 4.9%), silt (50.1 ± 5.6%), and clay (23.5 ± 2.6%) content. Moreover, the High Subsidence Region (HSR) cores yield an average sand (22.3 ± 9.1%), silt (45.9 ± 6.4%), and clay (31.5 ± 9.7%) content, respectively (Error shows as 1σ).

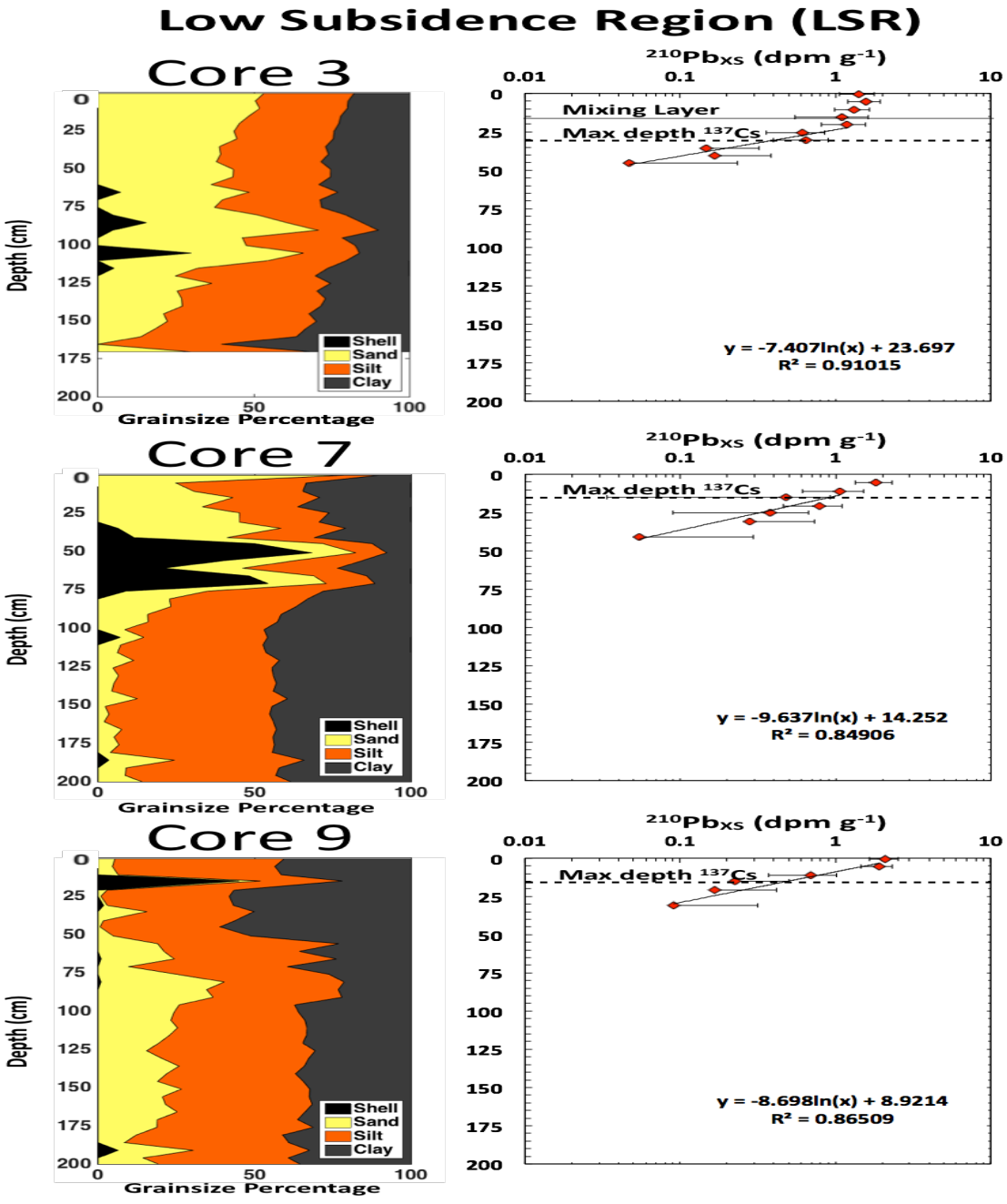

Figure 2.2 Representative example of low subsidence region cores (Core location are shown in Figure 2.1). Left panel indicate relative perentage of grainsize. Right panel displays unsupported ^{210}Pb activity ($^{210}Pb_{xs}$) in dpm g^{-1}. Regression lines for $^{210}Pb_{xs}$ and R^2 are shown within the plot. Dashed line indicates the depth of maximum ^{137}Cs activity. Solid line indicate the mixing layer depth. Note: depth scale is constent in Figures 2.2, 2.3, and 2.4, with plotted data indication depth of core.

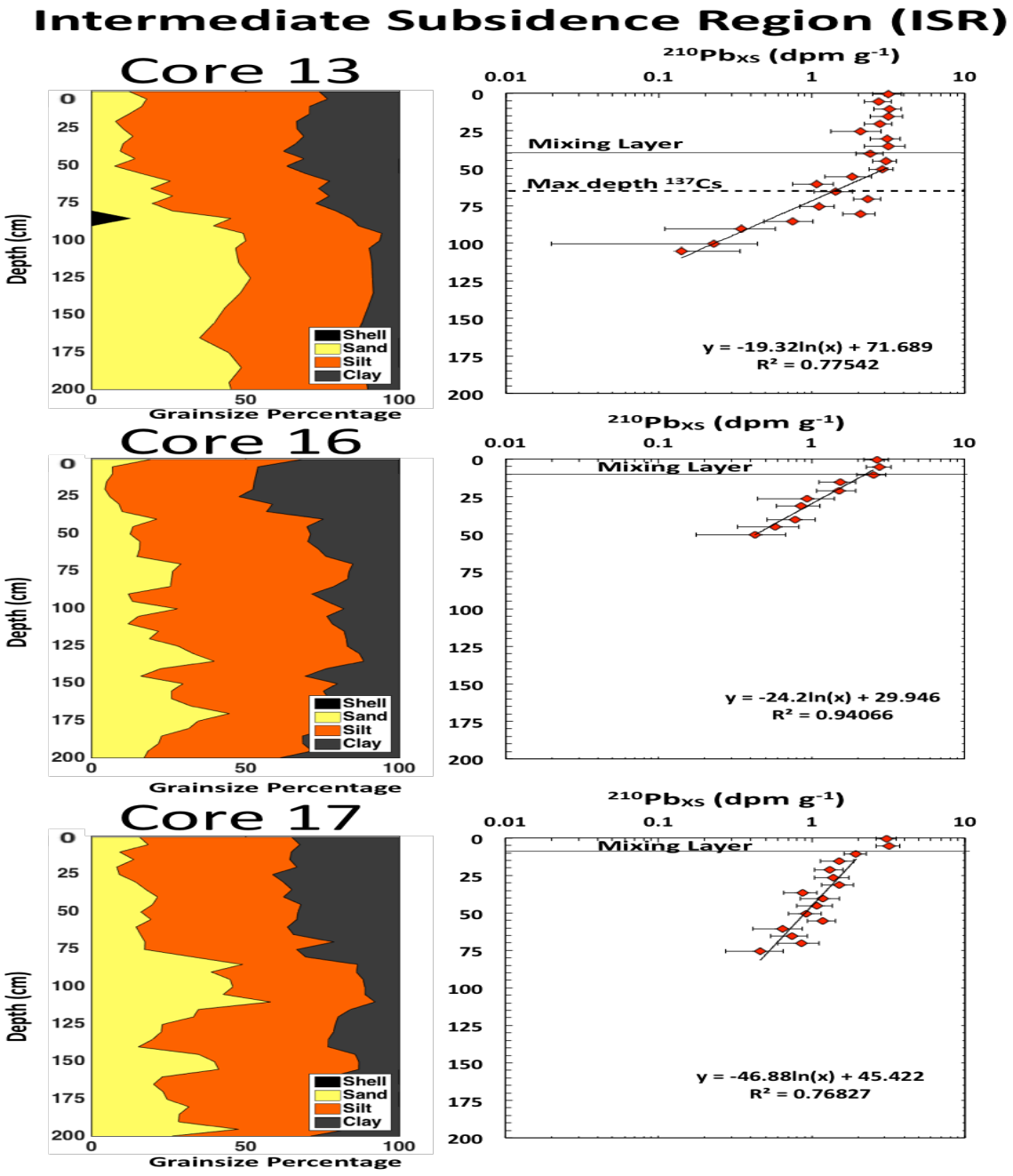

Figure 2.3 Representative example of intermediate subsidence region cores (Core location are shown in Figure 2.1). Left panel indicates relative perentage of grainsize. Right panel displays unsupported ^{210}Pb activity ($^{210}Pb_{xs}$) in dpm g^{-1}. Regression line for $^{210}Pb_{xs}$ and R^2 are shown within the plot. Dashed line indicates the depth of maximum ^{137}Cs activity. Solid lines indicate the mixing layer depth. Note: depth scale is constent in Figures 2.2, 2.3, and 2.4, with plotted data indication depth of core.

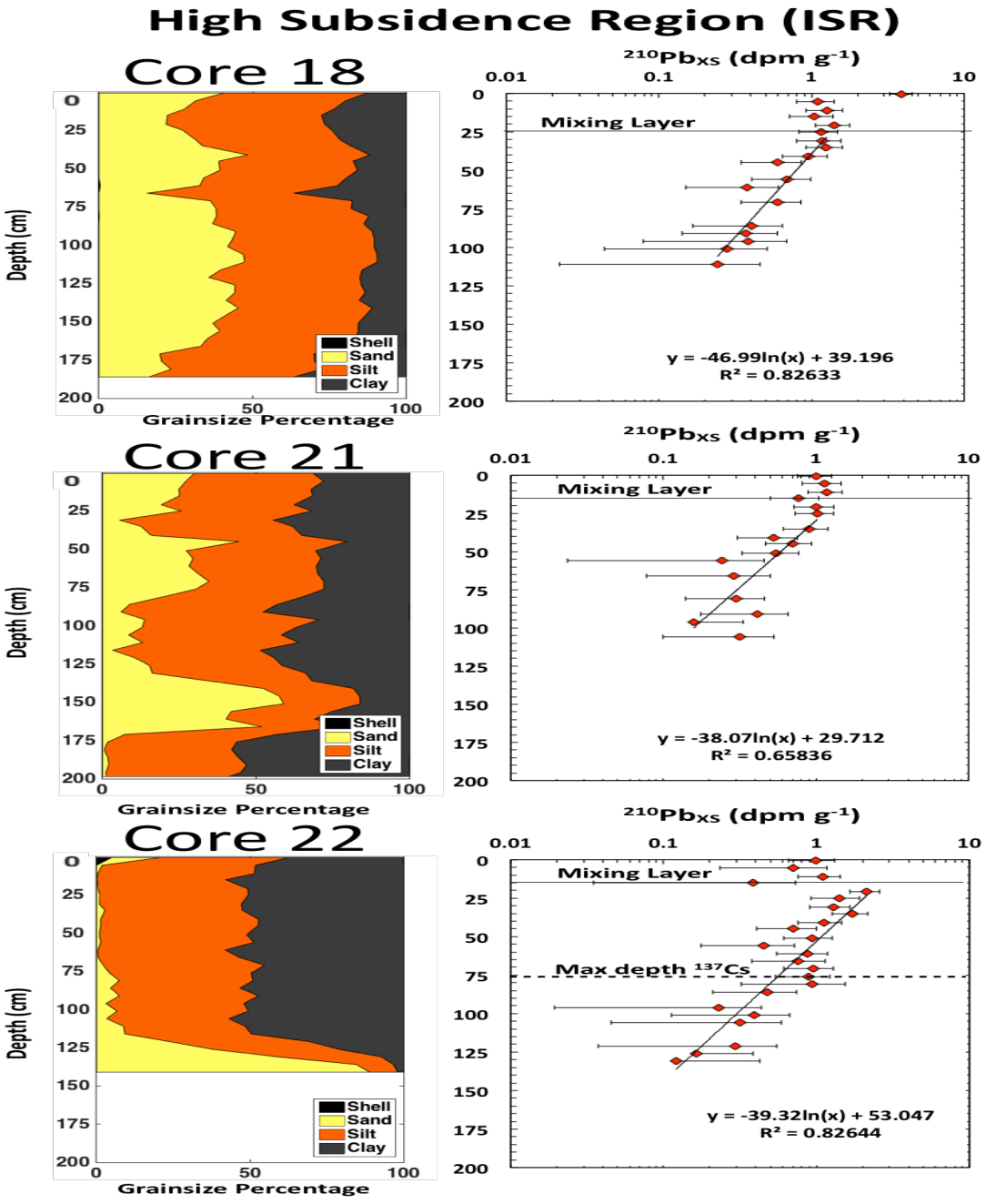

Figure 2.4 Representative example of high subsidence region cores (Core location are shown in Figure 2.1). Left panel indicates relative perentage of grainsize. Right panel display unsupported ^{210}Pb activity ($^{210}Pb_{xs}$) in dpm g^{-1}. Regression lines for $^{210}Pb_{xs}$ and R^2 are shown within the plot. Dashed line indicate the depth of maximum ^{137}Cs activity. Solid lines indicate the mixing layer depth. Note: depth scale is constent in Figures 2.2, 2.3, and 2.4, with plotted data indication depth of core.

2.5 Discussion

2.5.1 Impact of land subsidence

Several studies have concluded that estuaries may persist for a long period of time despite elevated RSLR if sediment accumulation rates balance or exceed the additional accumulation space created (Day et al., 1999; Morris et al., 2002; Rybczyk and Cahoon, 2002; White et al., 2002). In Galveston Bay, groundwater withdraw is the predominant cause of land subsidence, vastly exceeding tectonic subsidence rates (Coplin and Galloway, 1999) and differential compaction. The extensive groundwater removal to support petrochemical industries and an expanding population enhanced sub-surface geostatic pressure and caused clay lattices to compact, resulting in elevated land subsidence (Bawden et al., 2012; Kasmarek et al., 2012). In the early twentieth century, the area experienced a growth in population as a result of the discovery of oil, opening the San Jacinto River section of the Houston Ship Channel (SJR-HSC) in 1914, initiating industrialization along its banks. Until 1943, the area developed relatively slowly and subsidence was primarily localized, reaching a maximum of 0.18 m (0.48 cm yr^{-1}) (Coplin and Galloway, 1999; HGSD, 2013). After the 1940s, subsidence accelerated and extended spatially due to the rapid growth in population and industrial development; ultimately leading to approximately 3m of total subsidence during the 20th century (HGSD, 2008). Kolker et al. (2011) indicate that fault slipping due to groundwater extraction may have played a major role in the enhanced subsidence. Moreover, there is likely an additional natural subsidence component due to sediment compaction, addressed in section 5.3.

Combined with ESLR, these high rates of land subsidence contribute to RSLR. The RSLR varies considerably within Galveston Bay, and may be classified into three regions (Table 2.2). Evaluating tidal gauge records and national geodetic survey benchmarks provides estimated rates of local subsidence. With the noted exception of the Pier 21 Tidal Gauge, located within the Galveston Ship Channel, over the Incised Trinity River incised valley (Figure 2.1), which reveals a RSLR rate of 0.634 cm yr^{-1} between 1908 and 2014 (NOAA, 2013), there is a paucity of data within this region. During this time period, the estimated subsidence rate at Pier 21 of approximately 0.44 cm yr^{-1} contributes nearly 70% of the total RSLR. Near the eastern portion of West Galveston Bay, centered over the Texas City Refineries, there is area of localized elevated subsidence. This elevated subsidence that has been attributed, along with wave action and insufficient sediment supply, to significant salt marsh loss and erosion in the region (Ravens et al., 2009; White and Tremblay, 1995; White et al., 2002). Centennial average RSLR rates of 1.98 ± 0.15 cm yr^{-1} and 2.25 ± 0.18 cm yr^{-1} were estimated in ISR and HSR, respectively (Error shows as 1σ).

Recently, the withdrawal of groundwater within the regions of highest subsidence has been strongly regulated, resulting in an overall reduction in subsidence rates (Kolker et al., 2011; USGS, 2002; Zilkoski et al., 2006). In 1954, groundwater extraction was temporarily reduced when the surface water from Lake Houston supplemented the supply. The most dramatic reduction in groundwater pumping occurred in 1977, as the majority of water utilized for the industrial sector began to be sourced from Lake Livingston (Coplin and Galloway, 1999). Due to decelerating

subsidence rates, White and Tremblay (1995) predicted that future wetland losses would be primarily the result of a reduction in sediment supply.

2.5.2 Sediment accumulation rate

The historical data obtained from USGS and HGSD documenting land subsidence rates for the last 100 years were compared with sediment accumulation rates obtained from ^{210}Pb and ^{137}Cs to determine whether sedimentation has kept pace with land subsidence (HGSD, 2008; USGS, 2002). Sediment accumulation rates show a gradient with the highest rates in SJR/HSC, and decreasing both seaward (along salinity gradient) and towards LSR (Figure 2.1). Within HSR, sediment accumulation rates are comparable to previously reported results by Yeager et al. (2007), ranging between 1 cm yr^{-1} to 2.6 cm yr^{-1}. Sediment accumulation rates for LSR (Core 9) are approximately 0.29 cm yr^{-1}, which are equivalent to previously published rates of 0.29 cm yr^{-1} (Santschi et al., 2001) and 0.44 cm yr^{-1} (Yuill, 1991) for nearby cores. Moreover, the sediment accumulation rate in West Galveston Bay was determined to be 0.2 cm yr^{-1} Ravens et al. (2009), which is comparable to the average sediment accumulation rate, determined by this study for West Bay (0.3 cm yr^{-1}).

2.5.3 Subsidence over the Trinity and San Jacinto River Incised valley

In addition to eustatic sea level rise and the localized subsidence driven by fluid withdraw, within the portions of the bay which overly the Trinity and San Jacinto River incised valley (Figure 2.1), there is subsidence driven by differential compaction of the

Holocene valley fill. The Holocene valley fill is up to 30 m thick consists largely of unconsolidated estuarine mud (Siringan and Anderson, 1993). The portions of the bay not occupied by the Trinity River incised valley are underlain by the Beaumont Formation, a hard, dense, indurated clay paleosol, found generally only a few meters below the bay bottom. As noted above, the NOAA Pier 21 tidal station, which is located on the bayside of Galveston Island, has collected a continuous hourly water level time series since 1904 and has recorded an average RSLR rate of 0.65 cm yr^{-1}(NOAA, 2013). Pier 21 sits over the Trinity River incised valley, so this rate reflects a combination of the eustatic sea level rise of approximately 0.2 cm yr^{-1} as well as subsidence. However, this area is distal from the localized subsidence driven by fluid withdraw and fluid withdraw likely is not a significant factor in this elevated subsidence rate. This rate is more likely a result of differential compaction of the 30 m of unconsolidated Holocene fill underlying this site. To estimate the subsidence due to this differential compaction, this was compared to core 3 site in western West Bay. In an unrelated study, we found that the Beaumont Clay at the Core 3 site in West Bay is only 1 m below the bay bottom (Laverty, 2014). The sediment accumulation rate at this site is 0.28 cm yr^{-1}. Assuming that sediment accumulation in West Bay is in balance with ESLR, then there is no elevated subsidence in this area due to differential compaction or fluid withdraw. Furthermore, East Bay is not located over the Trinity River incised valley and it is distal from localized subsidence as well. Subsidence data obtained from cores located in the East Bay are uncertain and could be associated with errors. Sediment accumulation rate

in core 7 is 0.3 cm yr^{-1}, and if we assume a balance with ESLR, then the subsidence rate in this region is due to the differential compaction.

2.5.4 Analyses of subsidence vs sedimentation

Although the general pattern indicates where subsidence rates are high (i.e., high RSLR) and sedimentation rates are also high there is not a linear trend with land subsidence (Table 2.2). In order to evaluate these differences, the relationship between sediment accumulation rate and RSLR was calculated as the accretionary difference (AD) (Table 2.2; Figure 2.5). The accretionary difference throughout the three regions range between -.05 to -1.28 cm yr^{-1} with negative values representing sedimentation rates lower than subsidence rates (i.e., deficit). All cores in the three subsidence regions show a negative AD. Statistic analyses (heteroscedatic T-test) reveal that there is a significant difference ($p < 0.01$) between LSR and ISR. However, no significant differences were observed between the ISR and HSR ($p = 0.94$).

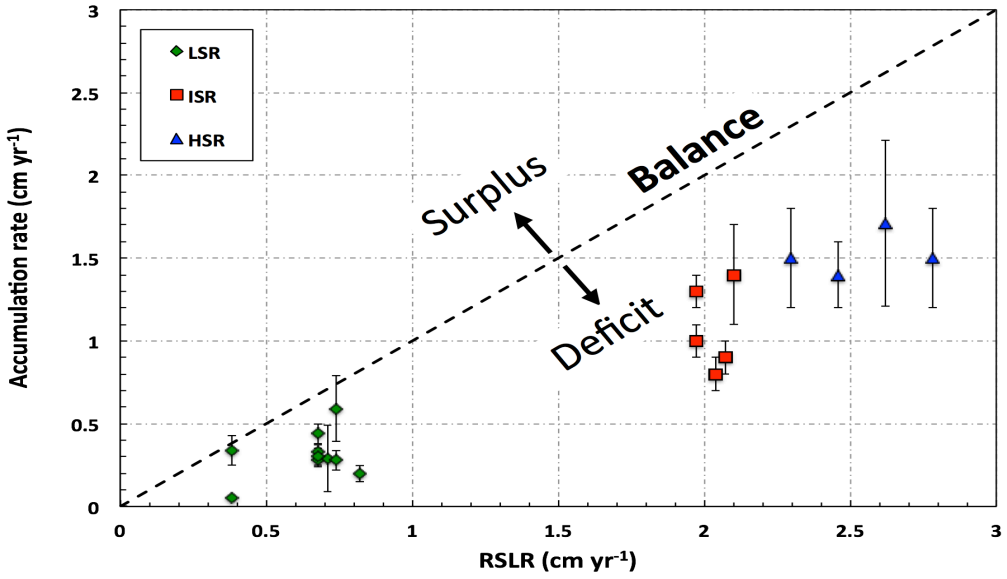

Figure 2.5 Relationship between sediment accumulation rate and Relative Sea-Level Rise (RSLR) in Galveston Bay. The dashed diagonal line indicates parity between sediment accumulation rate RSLR. Points lying below the line have an accretionary deficit whereas those above the lone have an accretionary surplus. Points are color coded according to the subsidence region.

It should be noted that the subsidence rates in figure 2.1 is from a limited data set and have been extrapolated across a large area. Consequently, the variations in agreement or disagreement between subsidence and accumulation rates within the defined subsidence regions may be, at least in part, a product of the errors associated with the extrapolation of the data rather than real differences. For example, in Trinity Bay, subsidence rates are calculated from land-based benchmarks along the western shore of Galveston Bay. Subsidence gradients are relatively low in this region; however, the subsidence was interpolated in this area based on data at least 25 km from coring

locations. Moreover, similar to Trinity Bay, the subsidence data calculated in the East and West bays are also obtained from a land-based benchmarks located in Texas City. The distance between the land-based benchmarks and the cores locations in the open bay makes the subsidence data obtained uncertain and many errors could be associated with such calculation. Changes in sediment transport within the bay and reduction in sediment supply may also be a factor in the deficit in sedimentation in some areas of the bay. Along the Trinity River, dam construction began in the upper portion of the drainage basin in 1911, and the Trinity River now has 31 major dammed reservoirs, including Lake Anahuac dam, completed within the bayhead delta of the Trinity River in 1954. The net affect has been a 50% reduction in sediment supply to the Galveston Bay (Ravens et al., 2009). In West Galveston Bay, the construction of the 8 km long Texas City Dike in 1915, which extends nearly the entire entrance between Galveston Bay and West Bay, has reduced the sediment transport into West Bay by blocking the eastern end to the West Bay (Anderson, 2007).

In Upper Galveston Bay, core 18 is located 1.3 km west of the portion of the Houston Ship Channel that extends through the open portion of Galveston Bay. Sediment transport dynamics in this region are mainly driven by the bow wakes of tankers, which causes scouring of the bay bottom to the west of the channel, and convergence of sediment within the ship channel, requiring nearly continual maintenance dredging. This enhanced scouring likely explains the 35% deficit in sediment accumulation compared to subsidence.

In Scott Bay, core 22 is in the middle of the petrochemical industry along the SJR/HCS as well as situated within the area of maximum subsidence. Lake Houston was formed when the San Jacinto Dam was completed in 1954 (Coplin and Galloway, 1999), 18 km north above Scott Bay, resulting in a significant decrease in the sand supply to the lower San Jacinto River. The +3 m of subsidence, coupled with the reduction in sediment supply, has resulted in a significant loss in wetlands and saltmarshes since 1944. The decrease in sediment supply likely explains why the sediment accumulation rate is 46 % lower than relative sea level rise.

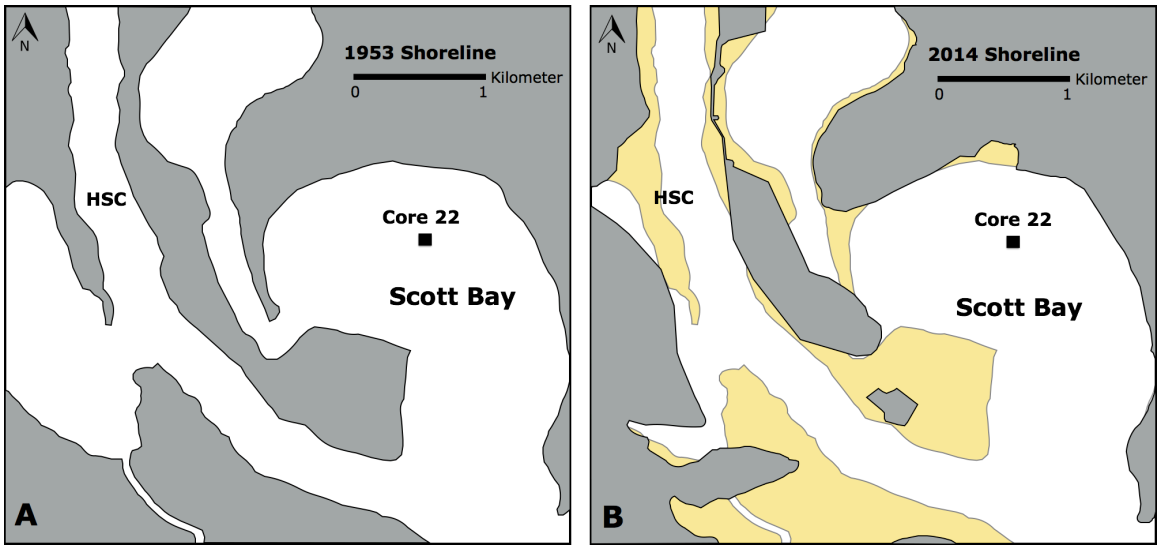

Figure 2.6 Loss in wetland and saltmarshes in Scott Bay, Houston Ship Channel (HSC). (A) The 1953 shoreline. (B) The 2014 shoreline, with the 1953 shoreline outlined in yellow.

Collectively, high rates of RSLR in addition to a reduction in sediment supply has ultimately led to an accretionary deficit, (Figure 2.5) which resulted in wetland loss and the conversion of land into open water, best illustrated in Scott Bay adjacent to the HSC-SJR (Figure 2.6). Furthermore, the results show that the volume of bay water is increasing due to localized anthropogenically driven subsidence along with rising sea-level and the reduction of sediment supply. This increase in volume will increase the fetch, and result in the strengthening of wave action and will increase and erosive processes (Kolker et al., 2011). Moreover, the surface area of the bay will increase the tidal prism, which will increase tidal energy, and wetlands loss will continue to increase (Lester and Gonzalez, 2002). The final results of this study are consistent with other studies were the RSLR is exceed sediment accumulation rate. For example, in New England the RSLR is 0.3 cm yr^{-1} for the last 100 years and the sediment accumulation rate is between 0.2 and 0.25 cm yr^{-1} and as a resulting in a deficit with respect to RSLR (Donnelly and Bertness, 2001). Other studies published sedimentation rates are higher than RSLR (Nichols, 1989). Williams et al. (2013) determined the sediment accumulation rate in the Nakdong Estuary of 5 cm yr^{-1} and the approximate sea level rise is 0.2 cm yr^{-1}. The accumulation rate in this region of the world is higher than required for equilibrium, resulting in a surplus within the estuary.

2.6 Conclusions

Modifications in the forces contributing to estuarine equilibrium, such as RSLR and sediment accretion rate, lead to an inundation regime and shift in grain size distribution. In Galveston Bay, sedimentation studies indicate higher sedimentation rates in SJR/HSC area and decreasing rates toward the GOM. Sedimentation rates are high in areas with higher land subsidence rates, although the sedimentation rates are lower than subsidence rates. However, when relative sea level rise is factored in, sedimentation generally did not keep pace with RSLR, although they have the same relative order. The results of this study demonstrate that RSLR rates, which are ranging from 40% and 55% are higher than sedimentation rates. Although the reasons for these differences vary between sites and the error associated with estimations of land subsidence rates vary depending on the distance from monitoring stations, it appears that in general, sedimentation is lagging behind RSLR.

Anthropogenic activities in GB show that subsurface activities such as groundwater withdrawal affect the surface sedimentary processes. Moreover, the study shows than the future management strategies should consider ameliorating the recent reduction in sediment supply. Galveston Bay is vulnerable to climate change due to the increase rate of RSLR, lower sedimentation rate, and low-lying coasts.

CHAPTER III

CENTENNIAL RECORD OF ANTHROPOGENIC IMPACTS IN GALVESTON BAY: EVIDENCE FROM TRACE METALS AND BIOMARKERS

3.1 Introduction

Over the past two centuries, anthropogenic activities have increased along major estuarine systems around the world (Barusseau et al., 1998; Bianchi, 2007; Day et al., 2013; Gao et al., 2012a; Kennish and Paerl, 2010; Williams et al., 2014; Yeager et al., 2010). The rate and degree of the impacts of these activities is expected to increase as a result of rapid population and industrial growth (Donnelly and Bertness, 2001; Williams, Dellapenna, et al., 2015; Williams, Lee, et al., 2015). Moreover, with increasing vessel size it is expected harbors will expand and navigation channels will be dredged to greater depths (Solis and Powell, 1999). Globally, this extensive urbanization and industrialization has led to severe alteration to estuarine systems (Byun et al., 2004; Santschi et al., 2001; Williams et al., 2013). Additionally, numerous chemical contaminants, including heavy metals, hydrocarbons, and pesticides, have been introduced to the water column through point and non-point pollution pathways, as well as atmospheric fallout (Choi et al., 2015; Ravichandran et al., 1995; Santschi et al., 1999; Santschi et al., 2001; Wen, shiller, et al., 1999; Williams, Dellapenna, et al., 2015; Yeager et al., 2007). Once accumulated within estuarine sediments, these chemical contaminants have a long residence time, resulting in degraded sediment quality. Thus,

benthic organisms are highly susceptible and typically initiate bioaccumulation up the estuarine food chain (Dellapenna et al., 1998; Kennish and Paerl, 2010; Long, 2000). If ultimately accumulated in the human body through ingestion of seafood, these chemical contaminants can be toxic and can cause serious chronic or sub-lethal effects (Day et al., 2013).

The distribution of chemical contaminants (Hg, Pb) and biomarkers (lignin) in sediment cores from industrialized and urbanized estuaries can be utilized as an indicator of past and present contamination events. Numerous studies have employed these tracers to evaluate shifts in organic matter signatures, particularly the enhanced accumulation of terrestrially derived materials (Brandenberger et al., 2008; Louchouarn and Lucotte, 1998; Louchouarn et al., 2006; Williams et al., 2014). Specific biomarkers such as lignin, which is the second most abundant biopolymer in vascular plants, constitutes a major source of terrigenous organic matter (TOM) to aquatic systems. On the other hand, anthropogenic input of lignin by-products from pulps and paper mills contribute substantially to a certain coastal systems (Brandenberger et al., 2008; Brandenberger et al., 2011; Louchouarn et al., 1999). The Galveston Bay (GB) system (Figure 3.1) provides valuable ecological and economic resources, and it is a prime example of an estuary that has been subjected to significant anthropogenic alteration over the last 150 years. The area surrounding the Houston Ship Channel (HSC) is intensely industrialized with chemical and petrochemical plants. GB is the seventh largest estuary in the United States (USA) and includes the (HSC) the busiest marine shipping lane in North America (Dellapenna et al., 2006). Moreover, the Port of Houston is the second largest port in the

USA, the eighth in the world, and with the highest foreign tonnage in the Americas (PHA, 2016). The GB watershed contains Houston, the fifth largest metropolitan area in the USA. Additionally, one-third of the US petroleum refining capacity is located along GB shores, along with numerous and diverse associated chemical industries (Santschi et al., 2001). The marine ecosystem of GB generates ~$19 million annually from its harvest of seafood, including ~10% of the US wild oyster harvest (EPA, 2007; Lester and Gonzalez, 2011). Clear Lake (Figure 3.1), in contrast, reflects the influence of significant urbanization rather than industrialization, when compared to the HSC. The National Aeronautics and Space Administration (NASA) in 1961 chose this region for its Lyndon B. Johnson Space Center. In 1974, the population was 16,000, and has increased to approximately 140,000 (Greene, 2016).

The proximity to these industries has resulted in extensive anthropogenic environmental impacts, including, groundwater extraction that resulted in over 3 m of subsidence in the upper bay and HSC since 1900 (Coplin and Galloway, 1999; USGS, 2002), poor air quality due to atmospheric fallout of particle bound contaminants (Lan et al., 2015), and substantial contamination of soil/sediment (Morse et al., 1993; Santschi et al., 2001; Wen, Santschi, et al., 1999). Hg is one of the most detrimental global aquatic contaminants (Bank, 2012; Liu et al., 2012). In marine environments, it can bioaccumulate and contaminate seafood, and pose a human health hazard (Di Leonardo et al., 2006). There are many natural and anthropogenic sources of mercury in the environment. Natural sources include volcanic eruptions and weathering of mercury bearing rocks (Bank, 2012). Anthropogenic emissions primarily come from coal

combustion, fossil fuels, metal (particularly gold) production, medical incineration, cement production, and local waste combustion (AMAP/UNEP, 2008; Bank, 2012; Liu et al., 2012).

Despite the urbanization and industrialization of the region, the recent concentration of trace metals (e.g. Hg) in the open waters and surface sediment are low, and the GB system is no longer considered a greatly polluted system with the exception of the Houston Ship Channel (Santschi et al., 2001). However, previous studies have only focused on surface and shallow sediments (≤10 cm deep), and thus have only investigated at maximum the last few decades (Harmon et al., 2003; Morse et al., 1993). The fate and transport of Hg in GB is poorly understood, as well as the historic organic matter signature (Santschi et al., 2001; Wen, Santschi, et al., 1999). Therefore, the aim of this research is to: 1) reconstruct the historical input of Hg and other trace metals in the system through sediment core analyses 2) determine the spatial distribution of Hg in GB, 3) calculate Hg inventories for the last 100 years and present Hg fluxes, 4) assess the degree of contamination and calculate the recovery rates, 5) assess the use of Hg as a supporting geochronological tool, 6) determine how anthropogenic activities affect the sedimentary organic matter signatures, and 7) to assess long-term policies and their influence on reducing the impact of environmental changes. Due to the industrial and residential importance of the GB watershed, these results clarify the fate and transport of organic biomarkers, Hg, and other particle bound contaminants under varying sedimentation regimes, and aid in local environmental management strategies to minimize impact to public health.

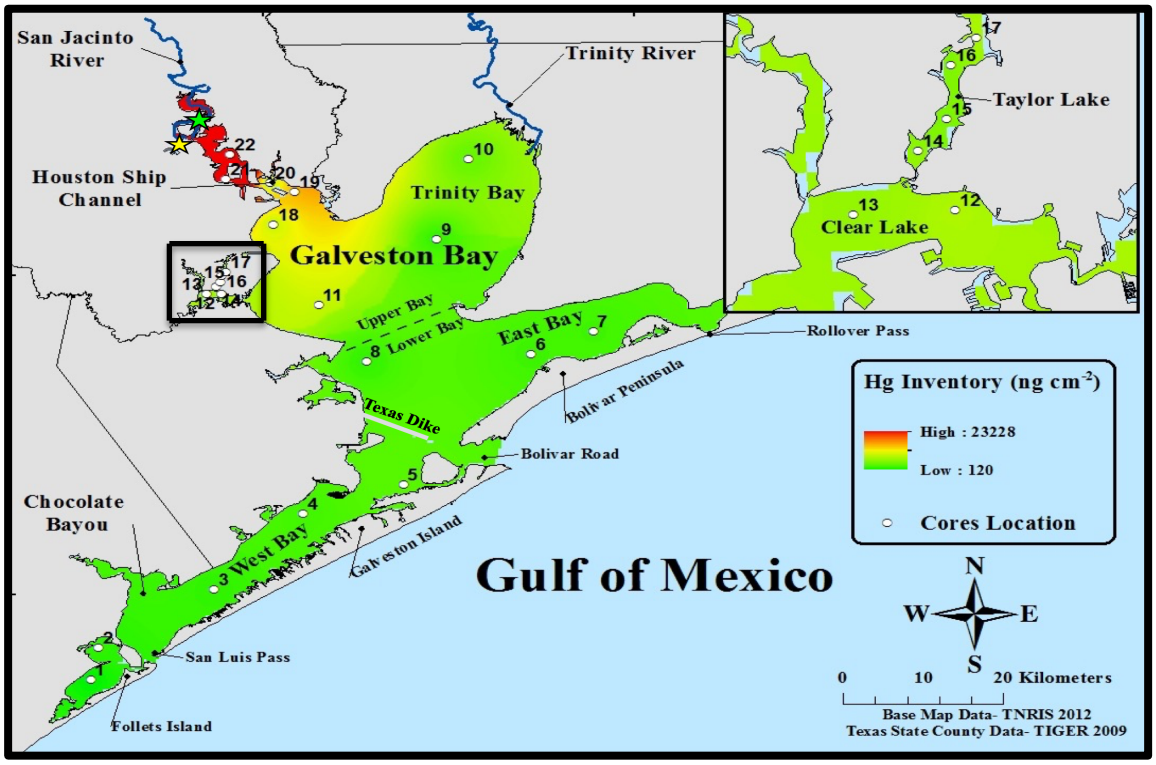

Figure 3.1 Study area map showing core sampling locations and interpolated Hg inventory for the last 100 years in Galveston Bay. The yellow star is the location of the Chlor-Alkali plant. The green star is the location of the waste pits site in San Jacinto River.

3.2 Material and methods

3.2.1 Data collection and core processing

A total of 22 sediment vibracores were collected on five cruises (June 15, July 27, August 1 and 8, 2012, and April 30, 2014) from Galveston Bay using 7.6 cm diameter aluminum core barrels (Figure 3.1). Cores were sealed immediately and subsequently stored at 4°C for further processing and analyses. Subsamples were collected at 5 cm intervals and the subsamples were homogenized, and stored in labeled Whirl-Pak bags until further processing. Two cores (Core 13 and 22) were selected for $\delta^{13}C$ and $\delta^{15}N$ analyses, XRF analyses, lignin analyses, radioisotopes analyses based on the location of the cores.

3.2.2 X-Radiograph

The X-radiographs of the sediment cores were taken using a MinX-Ray HF100+ Amorphous Silicon Imaging System 4030R, X-Ray unit at an energy level of 60 keV exposure time of 1/20 seconds.

3.2.3 Grainsize analyses

Grainsize distributions were determined using Malvern Mastersizer 2000 laser particle diffractometer. About 2-4 g of the wet samples were homogenized, sieved at 2 mm, and sonicated with sodium hexametaphosphate as a dispersant solution for 30 minutes at 25 ◦C and frequency of 40 kHz. The larger fractions of the samples were dried to determine the final grain size distribution. The instrument measured the fraction of sand, silt, and clay in triplicate and results are reported as an average.

3.2.4 X-Ray fluorescence

Downcore record of element abundant was determined using X-ray fluorescence (XRF) on two selected cores using a third generation AvaaTech XRF Core Scanner. The measurements were made every centimeter for the length of the archived section of the cores. The XRF measurements were made at energies of 10 keV and 30 keV, using a multichannel analyzer with a spectral resolution of 2048 channels at 20 eV/channel.

3.2.5 Radioisotope analyses

Activity of radioactive ^{137}Cs ($t_{1/2}$ = 30 yr, Eγ= 662 KeV) were measured using CANBERRA High-Purity Germanium (HPGe) well detector coupled with a DSA-1000 16 K integrated multi- channel analyzer. ^{137}C is used as an impulse tracer and it is anthropogenically introduced into the environment via the atmospheric testing of nuclear weapons. In 1963, extensive nuclear testing caused a well establish peak of ^{137}Cs in the sediment profile (Santschi et al., 1999). Using an identical geometry for gamma assay, the net counts of dry samples were converted to activity by using the efficiency factor. It is always assumed that it has a very short residence time in the water compared to it is half-life time, and that they are absorbed onto fine-grained particles (Dellapenna et al., 2003; Nittrouer et al., 1979).

3.2.6 Total organic carbon

Bulk sediments were analyzed for bulk organic carbon (%TOC) by combustion using a Costech Analytical Technologies, Inc. ECS 4010 CHNSO element analyzer.

Prior to analyses, carbonates were removed by acidifying the sediment with at least 2 ml of 1 N HCl added in plastic vials. After adding the acid, the vials were allowed to stand for about two hours at room temperature followed by drying at 60°C for 24 hours in the oven. The instrument was calibrated with acetanilide followed by NIST SRM 1941b (Organics in marine Sediment), which was used as verification standards. The NIST SRM 1941b and duplicate sediment samples were analyzed every 10 samples to insure accuracy and precision. The precision of replicate analyses of selected samples (n = 3) was < 2%.

3.2.7 Total mercury analyses

For the analyses of total mercury concentration (T-Hg) in the sediments, approximately 100 mg of dry and homogenized pulverized sediment samples at 5 cm intervals were analyzed using Direct Mercury Analyzer (DMA-80, milestone srl, Italy) which is complaint with U. S. EPA Method 7473 (EPA, 1998). The DMA-80 was calibrated using prepared standard solutions of mercury and the calibration curve was verified with Certified Reference Materials (CRM). In order to ensure precision, reliability, accuracy and consistency of the sediment samples for the total Hg, three Certified Reference Materials (CRM) (MESS-3 Marine sediment (0.091 ± 0.009 ppm, National Research Council of Canada), NIST 2702 Inorganics in Marine sediment (0.4474 ± 0.0069 ppm, National Institute of Standards and Technology), and PACS-2 Marine sediment (3.04 ± 0.2 ppm, National Research Council of Canada)) were used representing a different Hg range. Once the instrument was calibrated with liquid

standard solutions, the calibration curve was verified with the three CRM. Certified Reference Materials (CRM), blank to ensure no Hg is carried over the samples and duplicates to check the reproducibility were analyzed every 10 samples to ensure accuracy. The results obtained from the CRMs were excellent and in good agreement within the certified range with an average recovery rate for MESS-2 of 97 % ± 7 % (Mean ± RSD, n = 137), NIST 2702 (96 % ± 7 % (Mean ± RSD, n = 43), and PACS-2 (97 % ± 11 % (Mean ± RSD, n = 64).

3.2.8 $\delta^{13}C$ and $\delta^{15}N$

The HCl acidified sediment samples were analyzed for stable carbon and nitrogen isotopes at the Baylor University Stable Isotopes Laboratory by combustion with Costech Elemental Analyzer. International standard (USGS 40/41) was used for calibration. The standard delta notation (δ) of isotopic values is reported relative to Vienna Pee Dee belemnite (VPDB) for stable carbon and the atmospheric N_2 value for stable nitrogen. The standard deviation for the standard reference material was 0.02 ‰ and 0.05 ‰ for δ13C and $\delta^{15}N$, respectively.

3.2.9 Lignin analyses

Lignin-derived CuO oxidation products (LOP) were determined according to the method developed by Hedges and Ertel (1982) with modifications by Kuo et al. (2008) and Louchouarn et al. (2000). Briefly, the procedure involves the addition of homogenized ground sediment sample, providing 3-6 mg^{-1} OC, CuO oxidant (330 ± 4

mg), 150 ± 4 mg of $Fe(NH_4)_2(SO_4)_2 \bullet 6H_2O$, and a stainless steel ball bearing (ensures homogenization during oxidation) in a stainless steel mini reaction vessels (3 mL; Prime Focus Inc). If the carbon percentage is low (< 3mg OC for a normal sized sample) and there is not enough sample material, 5 mg of glucose was added as a sacrificial carbon source to minimize sample loss during oxidation. Each reaction vessel (n = 12) was then moved to a customized purging block (Prime Focus Inc.), and filled (~ 2.5 mL) with 2 N Ar-sparged NaOH solution (for 45 min to exclude molecular oxygen). For 45 minutes, the headspace of the reaction vessel was sparged with Ar and then closed. The reaction vessels were heated at 154°C for 3 hours in a customized Hewlett-Packard 5890 gas chromatograph. After cooling, 12 μg of trans-cinnamic acid (3-phenylprop-2-enoin acid) was added directly to each reaction vessel as a surrogate standard. The reaction vessels were then centrifuged to separate the solids and rinsing (2x) with X mL of 1 N NaOH. The aqueous solution was acidified with 6 N HCl (pH ≤ 1) and extracted with ethyl acetate (9 mL). Residual water was removed with Na2SO4 and, the extract was evaporated to dryness using a LabConoTM solvent concentrator. The residue was then re-dissolved in pyridine (400 μL) and further diluted with pyridine (50:200). A sub-sample was transferred to a 1.5 mL amber vial to which anisic acid was added and then derivatized with N,O-bis(trimethylsilyl)trifluoroacetamide (BSTFA) containing 1% trimethylchlorosilane (TMCS; Supelco, PA, USA) at 75°C for 30 minute before analysis by gas chromatography-mass spectrometry (GC/MS).

3.2.10 GC/MS analyses

A Varian Ion Trap 3800/4000 system filled with a fused silica column (VF 5MS, 30 m X 0.25 mm i.d., 0.25 μm film thickness; Varian INC.) was used for the quantification and separation of the trimethylsilyl (TMS) derivatives of CuO oxidation by-products. Samples were injected in splitless mode, into a straight glass liner inserted into GC injection port. He was used as the carrier gas (1.0 mL min^{-1}). The GC oven was operated from 65°C (2 min delay) to 300°C (held 5 min). The GC injector and the GC/MS interface were both maintained at 280°C. The MS was operated in the electron ionization (EI, 70 eV) using full scan. The identification of the compounds was performed using GC retention time and by comparing full mass spectra with standards. The instrument was operated under the full scan mode in the mass range m/z 50-500 and 1-3 ions were selected for quantification. Quantification was performed using a relative response factor (RRF) adjusted to the surrogate standard. The analytical precision of the CuO oxidation method used in the lab was validated from replicate analyses by the oxidation of reference standard estuarine sediment (NIST SRM 1941b). The replicate analyses of the NIST SRM 1941b showed excellent reproducibility with mean sample deviation of ≈ 5%.

3.3 Results and Discussion

3.3.1 Spatial distribution and historical reconstruction of contamination

3.3.1.1 Spatial distribution/ fluxes

Contaminated sediment can have a long-term effect on the ecological systems and, subsequently, human health. In the early 1900s, within the study area, sediment contamination, particularly of mercury, increased with refinery expansion, coincident with the growth in Houston's population (Harmon et al., 2003). In 1960, the EPA listed HSC as one of the top 10 polluted areas in the United States (EPA, 1980). Harmon et al. (2003) found that there was a uniform distribution of trace metals in the surface sediment in GB, with the exception of mercury (Hg), which was elevated in the HSC (200 ng g^{-1}), and about moderate (50 ng g^{-1}) elsewhere. Based on surface sediment obtained from the HSC since 1970, sediment quality has been shown to be improving, with the exception of Hg (GBST, 2016). Between 1970 and 2010, Hg concentration in surface sediments exhibited episodic spikes in several sub-bays and tributaries of HSC, reaching 9000 ng g^{-1}, 15000 ng g^{-1}, 8000 ng g^{-1}, 20000 ng g^{-1}, and 1000 ng g^{-1} in 1978, 2001, 2003, 2006, and 2010 respectively (Greene, 2016). Due to high Hg and other trace metal concentrations in the surface sediments, in 2002 the National Priorities List (NPL) identified sections of the upper HSC as a Superfund (CERSLA) site. Specifically, these sites include Patrick Bayou where a Chlor-Alkali plant is located (Figure 3.1) (Lester and Gonzalez, 2011), and the San Jacinto River waste pits (56656 m^2) (Figure 3.1), built in 1960s for disposal of pulp and paper mill wastes (EPA, 2015).

In this study, total Hg concentration in the surface sediment reflects both the

industrialization/urbanization gradient toward the Gulf of Mexico, following the salinity gradient of the bay. Hg concentrations found in surface sediments are within the previously reported range of 10 - 280 ng g^{-1} (Morse et al., 1993; Santschi et al., 2001). Surface Hg concentrations vary widely from site to site, ranging from between 6 - 162 ng g^{-1}, with an average of 50.0 ng g^{-1} (Table 3.1). These surface Hg concentrations exceed the background Hg concentrations in the upper Bay, which indicate anthropogenic input in that region. However, surface Hg concentrations in most sediment in West and East Bays are still within background values (Table 3.1). In West Bay, the Texas Dike (Figure 3.1) blocks sediment transport from the open bay, which resulted in decreased sedimentation rates and thus contamination in this region (Anderson, 2007). Additionally, the lower T-Hg value in East Bay is a result of a low sedimentation rate (Al-Mukaimi, 2016). In general, there is a decreasing gradient of T-Hg values from HSC toward the open ocean, with the exception of cores located in Trinity Bay and Clear Lake region (Figure 3.1), which record values higher than some core from HSC (Core 21, 20, 19, 18) (Table 3.1). Balogh et al. (1999) stated that urbanization could enhance the delivery of Hg to surface sediments from non-point sources such as sewage. This may explain why Clear Lake cores have higher surface Hg concentration than HSC where environmental regulations have been emplaced to reduce point sources. The present-day Hg fluxes (ng $m^{-2}yr^{-1}$) to the surface sediment were calculated using the following equation:

$$\text{Hg flux} = (1- \varphi) * S * \rho * \text{T-Hg}$$

where S is the sediment accumulation rate (cm yr^{-1}), T-Hg is the total Hg concentration

(ng g^{-1}), ρ is the sediment density (g cm^{-3}) and φ is the porosity (Table 3.1). The results show low fluxes of Hg in the lower bay (1 to 8 ng $m^{-2}yr^{-1}$) and moderate fluxes in the upper bay and Clear Lake region (6 to 18 ng $m^{-2}yr^{-1}$). On the other hand, in the upper part of the bay, especially within the HSC there is a high Hg flux (24 to 120 ng $m^{-2}yr^{-1}$). The elevated surface flux likely reflects the influence of the anthropogenic activities along HSC. The differences result from a combination of point sources input, sediment accumulation rate and atmospheric input from the petrochemical industry as well as coal combustion (Lan et al., 2015). Santschi et al. (2001) estimated the flux of Hg to surface sediment at 13.6 ng cm^{-2} yr^{-1} in Trinity Bay. The present-day flux of Hg in Trinity Bay is now at 6.1 ng cm^{-2} yr^{-1} (Table 3.1). The decrease in Hg fluxes over the last decade indicates a reduction in the amount of Hg being released due to continued environmental regulations.

Table 3.1 Average sediment accumulation rate (S_{Avg}), surface Hg concentrations (S-Hg), background Hg concentration (Bkg-Hg), maximum Hg concentration (Max-Hg), depth of the maximum Hg concentration represent the period between 1960s and 1970s (Max-Hg depth), present-day Hg fluxes and Hg inventory for the last 100 years for Galveston Bay. N.D. not determined. * Average sediment accumulation rate from (Al-Mukaimi, 2016).

Region	Core	S_{Avg}*	S-Hg	Bkg-Hg	Max-Hg	Max-Hg depth	Hg flux	Hg Inventory
		(cm yr^{-1})	(ng g^{-1})	(ng g^{-1})	(ng g^{-1})	(cm)	(ng m^{-2} yr^{-1})	(ng m^{-2})
West Bay	1	0.05	16	8	22	5.5	1	120
	2	0.34	10	8	15	10.5	4	445
	3	0.28	18.5	8	22	15.5	5	463
	4	0.33	20	12	31	150.5	8	692
	5	0.29	12	8	48	30.5	5	1038
East Bay	6	0.44	12	15	31	165.5	4	633
	7	0.30	6	18	30	5.5	3	649
Texas City	8	0.20	19	15	27	11	4	511
Trinity Bay	9	0.28	50.5	18	46	5.5	6	555
	10	0.59	48	20	48	0.5	11	1350
Upper Bay	11	-	45	20	57	11	N.D.	N.D.
Clear Lake	12	1.00	45	10	63	50.5	18	2825
	13	1.20	47	6	61	60.5	15	2285
Taylor Lake	14	-	25	10	33	5.5	N.D.	N.D.
	15	0.80	49	6	66	45.5	12	1704
	16	0.90	49	10	71	30.5	14	1811
	17	1.40	33	11	58	46.5	17	2798
Houston Ship Channel	18	1.50	19.5	9	104	61	25	3516
	19	-	7	8	97	131	N.D.	N.D.
	20	1.40	18	9	142	76	24	3331
	21	2.00	30	14	1313	106	40	21282
	22	1.50	162	8	2374	76	120	23228

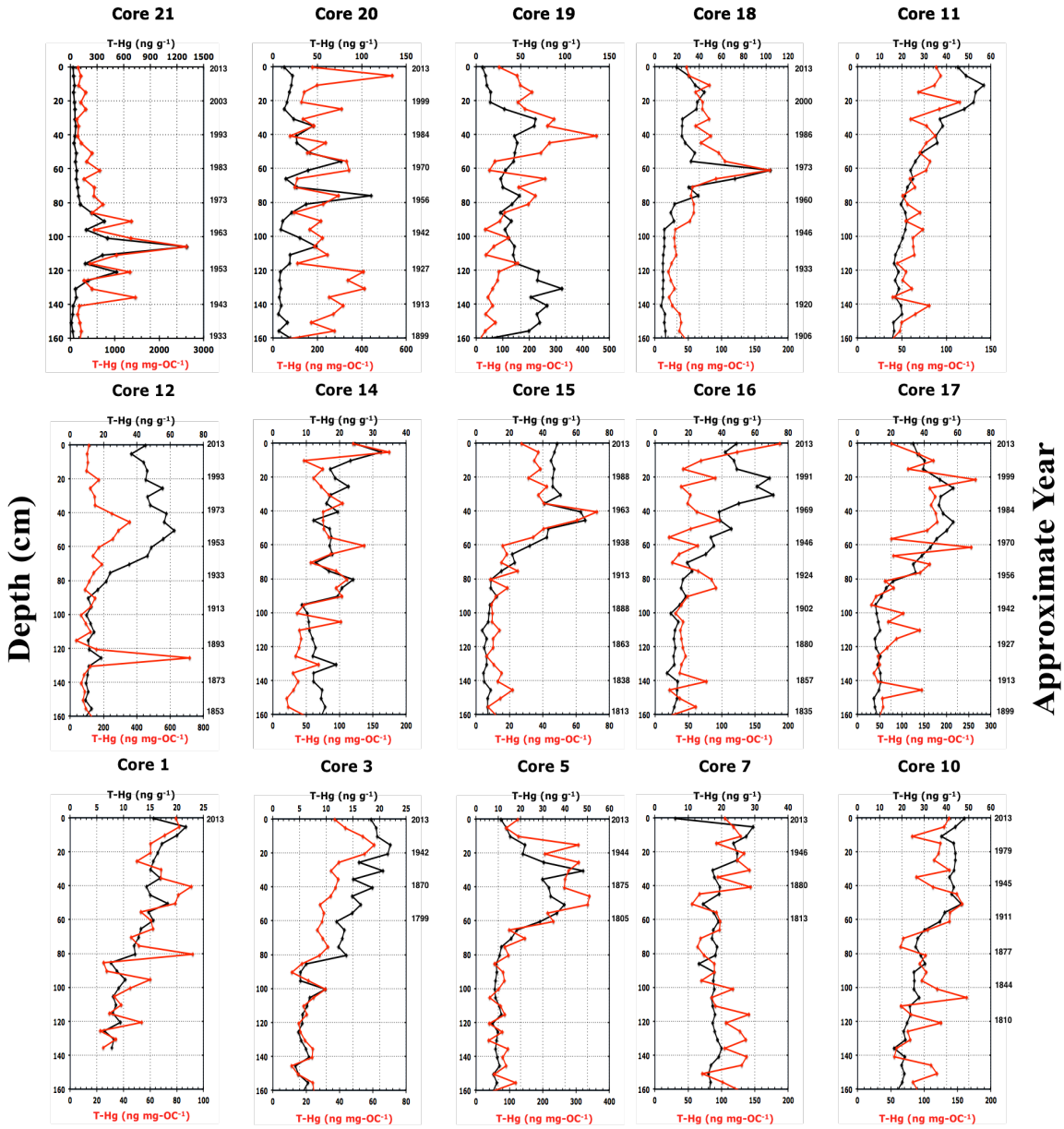

Figure 3.2 Profiles of bulk total Hg (black), and carbon normalized total Hg (red) for cores in Galveston Bay (left) and corresponding deposition are estimated from geochronology (Table 3.1) (right). Note scale difference. Note that core 19, 11, and 14 did not have geochronology data due to sediment mixing within the cores. Also note that the error in estimating geochronological dates greater than 150 years is greater both due to errors inhering in the geochronology technique as well as historical changes in land usage and consequently sediment accumulation rates (Core 1, 3, 5, 7, and 10). Core locations are display in Figure 3.1

3.3.1.2 Historical record and inventory of trace metals

The historical reconstruction of contamination from sediment cores helps to assess the effectiveness of past environmental regulations, and aid in improving future management strategies (Brandenberger et al., 2008; Ravichandran et al., 1995). In Galveston Bay, variations in T-Hg concentration with depth correspond to the historical input of anthropogenic T-Hg (Figure 3.2, 3.3, and 3.4). Most T-Hg profiles can be separated into two distinct groups, representing pre- and post-contamination (Figure 3.2, 3.3, and 3.4). Comparing these two groups reveals a significant difference ($p < 0.001$) (heteroscedastic t-test), with the exception of core 19 ($p > 0.001$), which could be explained by sediment mixing. Studies show that Hg related to anthropogenic inputs is associated and forms stable complexes with organic matter (Acquavita et al., 2012; Louchouarn and Lucotte, 1998; Williams, Dellapenna, et al., 2015). TOC was analyzed as a proxy to organic matter abundances to determine the relationship with T-Hg concentration (Figure 3.2). The reason is that Hg most strongly sorbs to thiols and sulfides. These profiles display similar trends to T-Hg, indicating that the reason for the T-Hg increase is due to increased source input and not an increase in carrier phase (TOC), which is similar to other studies (Louchouarn and Lucotte, 1998; Santschi et al., 1999; Williams, Dellapenna, et al., 2015).

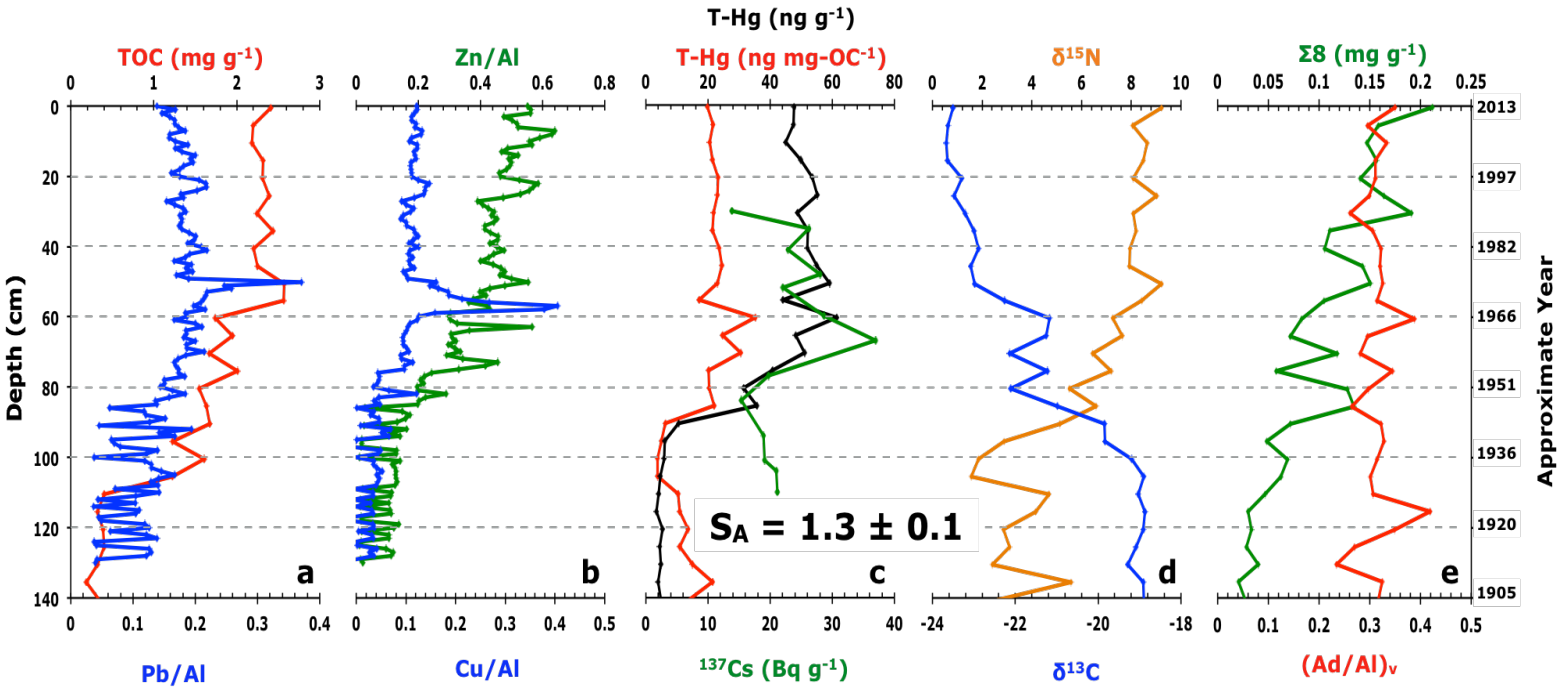

Figure 3.3 Detailed sediment core profiles for core 13 in Clear Lake. The sediment core plotted against depth (left) and corresponding deposition are estimated from geochronology (right). (a) Total Organic Carbon (TOC) and Pb normalized to Al. (b) Zn and Cu normalized to Al. (c) bulk total Hg, carbon normalized total Hg and ^{137}Cs activity. (d) Stable Nitrogen (N^{15}) and Carbon (C^{13}) isotopes. (e) Mass normalized (Σ8) yields of lignin oxidation products (LOP) and the ratio of vanillic acid to vanillin $(Ad/Al)_V$. The average sediment accumulation rate is indicated (S_A).

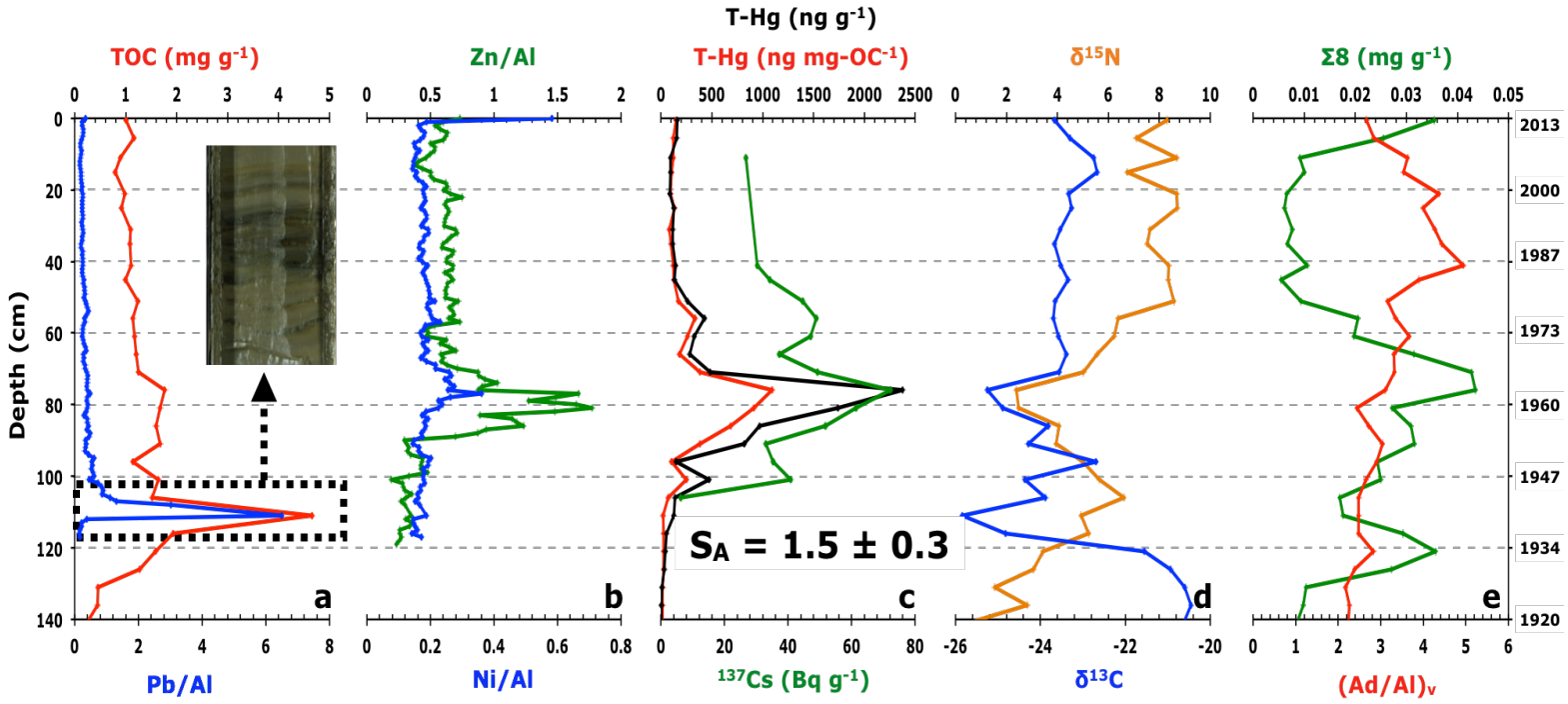

Figure 3.4 Detailed sediment core profiles and data for core 22 in Scott Bay in HSC. The sediment core plotted against depth (left) and corresponding deposition are estimated from geochronology (right). (a) Total Organic Carbon (TOC) and Pb normalized to Al with image of the core section associated with that depth. (b) Zn and Cu normalized to Al. (c) bulk total Hg, carbon normalized total Hg and ^{137}Cs activity. (d) Stable Nitrogen (N^{15}) and Carbon (C^{13}) isotopes. (e) Mass normalized ($\Sigma 8$) yields of lignin oxidation products (LOP) and the ratio of vanillic acid to vanillin $(Ad/Al)_V$). The average sediment accumulation rate is indicated (S_A).

The geochronological data (Table 3.1) were used to reconstruct the historical input of Hg in Galveston Bay. The increase in Hg concentration above background concentrations occurs approximately in the early 1900s, with a clear peak between 1960-1970s, followed by a decreasing trend. Starting in 1897 with the discovery of oil, the area experienced a rapid growth in population and industry, resulting in the opening of the San Jacinto River section of the Houston Ship Channel (SJR-HSC) in 1914, and development of industry along its banks. Groundwater pumping and oil extraction was extensive in the early 1940s to support the second World War (WWII; 1939-1945) (Coplin and Galloway, 1999) and is apparent in T-Hg profiles (Figure 3.2, 3.3, and 3.4).

Numerous studies in North America have shown that detectable chemical contamination in estuarine sediment began in the early 1900s, reached a maximum between 1940-1980s, followed by a steady decrease due to the reduction in point source input (Brandenberger et al., 2008; Brandenberger et al., 2011; Nitsche et al., 2010; Santschi et al., 1999; Valettesilver, 1993; Yeager et al., 2007). Studies within Europe and developed Asian countries show similar chemical contaminant trends in the sediment profiles associated with industrial development (Choi et al., 2015; Di Leonardo et al., 2006; Shi et al., 2010; Williams, Dellapenna, et al., 2015). In Galveston Bay, the sediment record seems to track the contamination trend in these regions. In all sites (Core 18, 19, 20, 21, 22) near the Chlor-Alkali plant (began operation in 1948), T-Hg profiles reveal maximum concentration between 1960-1970s (Table 3.1), at depths deeper (61-131cm) than previously sampled (Harmon et al., 2003; Santschi et al., 2001; Wen, Santschi, et al., 1999) The T-Hg peaks reach highest values in the HSC close to the

industrial point sources (i.e., Chlor-Alkali site) (Core 22; 2374 ng g^{-1}; Figure 3.4), which is 100 times surface/background values, and decrease in seaward direction (Core 18; 104 ng g^{-1}; Figure 3.2) and decrease dramatically toward the back barrier lagoons, to reach value between 15 to 48 ng g^{-1} in West and East Bay (Table 3.1). The maximum concentration is found higher in concentration with decreasing distance to the Chlor-Alkali plant (Figure 3.5a). On the other hand, the depth of maximum concentration is deeper corresponding with decreasing distance to the Chlor-Alkali plant with exception to core 19 where the mixing, likely caused by dredging and the higher sedimentation rate, in core 21 affect the depth (Figure 3.5b; Table 3.1) respectively. Moreover, Hg has been found to display non-conservative estuarine mixing behavior in the GB water column, decreasing exponentially towards the sea (with increasing salinity) (Han et al., 2006). Clear Lake and Taylor Lake T-Hg profiles show similar trends to HSC cores, but with lower concentration and no defined T-Hg peaks (Table 3.1; Fig 2, 3).

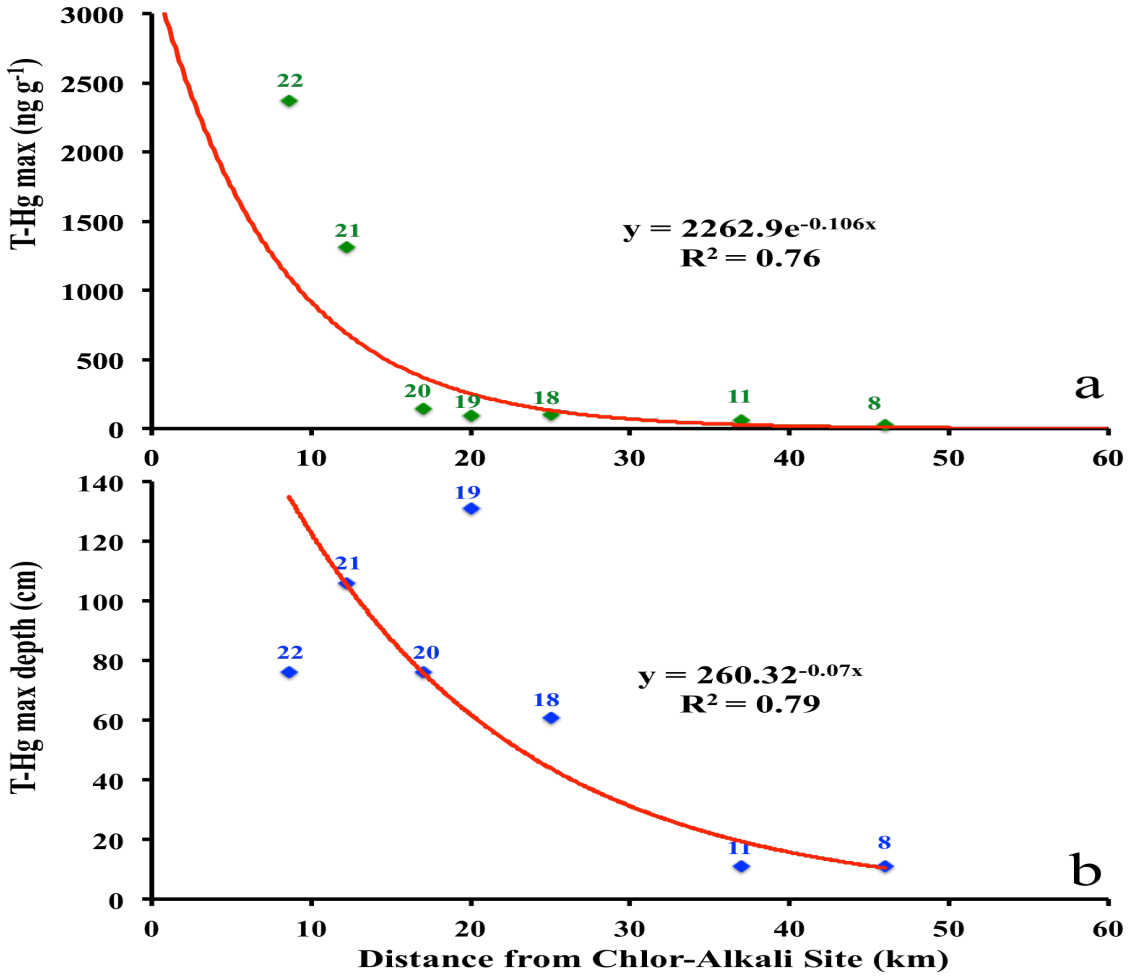

Figure 3.5 Maximum T-Hg concentration with distance from Chlor-Alkali site upper in HSC (a) and depth of maximum T-Hg concentration (b).

Furthermore, T-Hg inventory was calculated in Galveston Bay in order to estimate total anthropogenic input to the system throughout the last century (Figure 3.1; Table 3.1). T-Hg inventory (ng m^{-2}) represents the total amount of Hg being loaded to the sediment over a period of time and deposited over a surface area (Kolak et al., 1998). The following equation was used to calculate the amount of Hg buried in the sediment:

$$\text{Hg Inv} = \Sigma\,[\text{T-Hg} * (1- \varphi) * \rho * d]$$

Where d is the thickness of the sediment between consecutive depth intervals (cm). Results (Figure 3.1; Table 3.1) show a significant difference between areas around SJR/HSC and the southern side of the bay. The accumulation of total T-Hg is higher in SJR/HSC (23228 ng m^{-2}) and decreases to values between 120 and 1038 ng m^{-2} towards GOM (2169 ng m^{-2}). The distribution of anthropogenic inventories of T-Hg follows the same trend as T-Hg fluxes high in the upper section of the bay and decreasing seaward, indicating that most Hg is trapped in the upper part of the bay and the western side and less Hg has been deposited in East and West Bay. This observation supports the idea that, apart a coincidence of higher sources with higher sedimentation rates, in these locations high sediment accumulation rate and higher land subsidence (Al-Mukaimi, 2016) causes T-Hg concentration to be preserved and stored deeper in the sediment column in HSC, compared to locations where the land subsidence rate and sediment accumulation rate are low and where there is higher wave energy and coarser grain size fraction dominant. Additionally, these results support the idea that estuaries act as filters, trapping sediments, and less contamination is transported to open ocean systems (Dellapenna et al., 2003). Therefore, due to the high concentrations of T-Hg buried at depth (61-131cm), it is essential to minimize the dredging activities in previously undredged portions of the HSC area, because these areas contain the highest inventories of Hg at depth, and such dredging could release contaminants as the reduced sediments are exposed to oxic environments (Wen, shiller, et al., 1999). Other than the dredging activities, the nature of the particle mixing, whether biological and/or physical mixing

can have an effect on the fate and transport of contaminants in the system. For example, if dominated by physical mixing, the potential for the contaminants is high to be re-introduced in the water column and be spread over a larger area due to the physical mixing. On the other hand, biological mixing (bioturbation) has a greater potential for the contaminant to move to higher trophic levels and thus, for digestion by consumers (Dellapenna et al., 1998). The x-radiography of core 20 (Figure 3.6) shows there is an in-situ bivalve in the top 20 cm, which indicate a higher potential of the contaminants to be ingested by macrobenthic organisms. On the other hand, it seems that from the finely-lamination and clear T-Hg peaks in this core (HSC) that bioturbation and storm activities in these sediments did not prevent the burial T-Hg, with little distortion of the peak shape (Core 22, 21, 20, 18) in HSC.

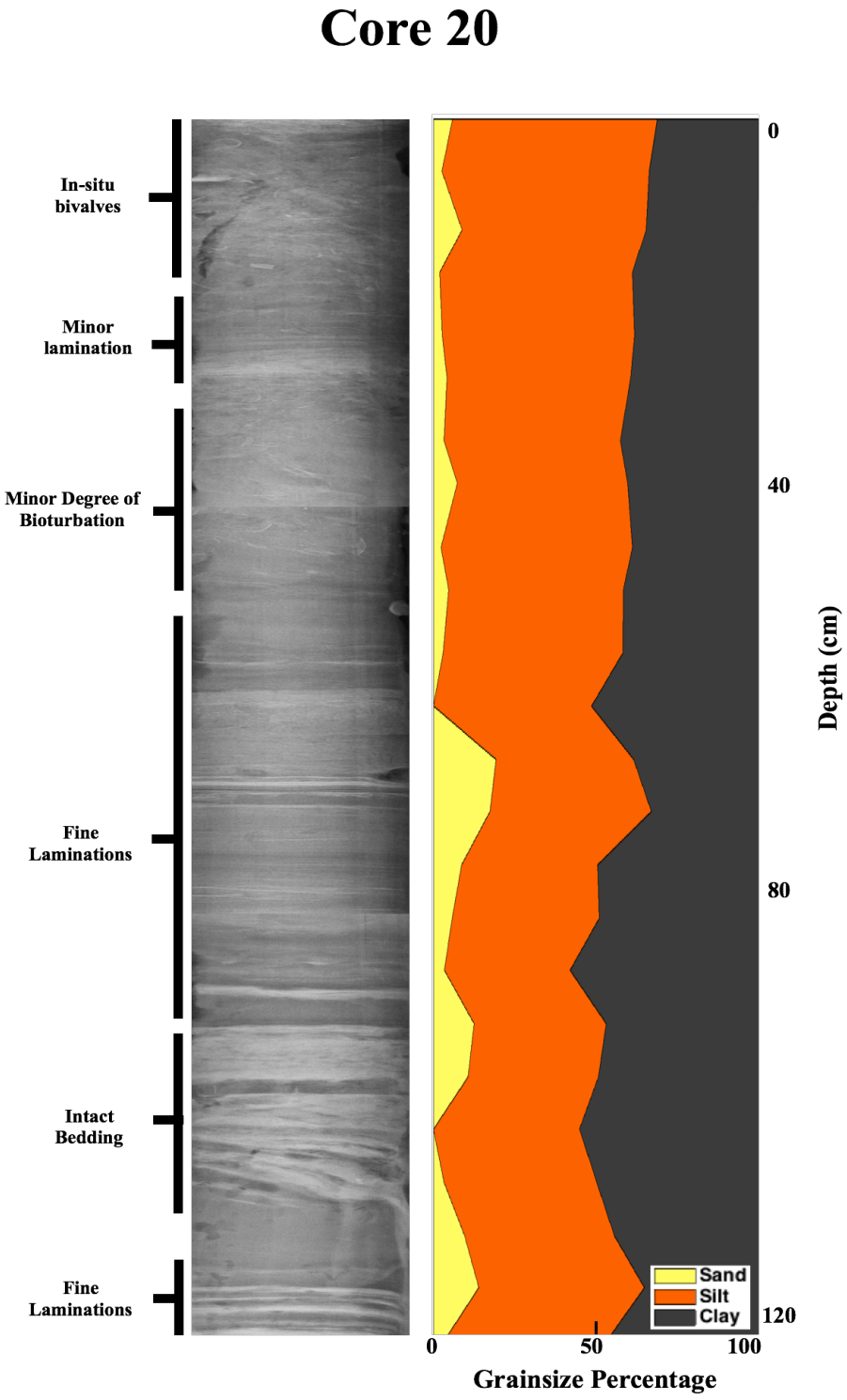

Figure 3.6 Representative X-radiography section of core 20 in HSC and grain size composition profile. Key features are indicated in the right and the depth (cm) in the left.

We have chosen to focus on two distinct cores for trace metal and biomarker signals (see section 3.2); one-representing the impacts related primarily to industrialization (core 22; Figure 3.2) and the other to urbanization effects (Core 13; Figure 3.3). Core 22 (Figure 3.4) is the core with the highest T-Hg concentration and has a higher Pb/Al ratio. XRF data have been normalized to Al because of its high natural concentration in trace metal - sorbing fine-grained sediments, to distinguish anthropogenic from natural element abundance. Lead (Pb) is a heavy metal that could cause similar problems as Hg to the ecosystem and humans (Clark et al., 1991). Beginning in the 1920s, Tetraethyl lead (TEL) was added to gasoline in the United States to increase combustion efficiency in high compression engines. Between 1950-1970s, there was a dramatic increase in TEL use, and after 1970s TEL use rapidly declined (Ravichandran et al., 1995). Core 22 shows that there is a well-preserved layer of Pb at depth between 100-120 cm between the 1930s-1950s, corresponding to an elevated TOC signal. Although we interpret this increase to TEL, further analyses ($^{206}Pb/^{207}Pb$) are necessary to elucidate the sources of Pb (Louchouarn et al., 2012). Qualitatively, when the core was split there was a distinct smell of gasoline in the reduced layer of contamination. Other trace metals such as Ni and Zn show a similar trend to the T-Hg profile (Figures 3.3 and 3.4). These two metals are used commonly in the electroplating industries and the production of alloys. In core 22, these trace metals (Pb, Ni, and Zn) show a decline in abundance after the 1970s. On the other hand, core 13 displays a similar trend to T-Hg, suggesting their initial elevated introduction beginning

around the early1940s when this region was residential and the contaminants were introduced through surface runoff. The Copper (Cu) profile shows a clear peak at about 1966 (60 cm) and decrease thereafter. Copper (Cu) is usually high in sewage treatment plants (Ravichandran et al., 1995).

Historical Hg sediment profiles have been utilized in several studies as a geochronological tool. It has been suggested under certain circumstances; T-Hg in the sediment could be more widely incorporated to recent sedimentary processes (<200 yrs) due to the lower cost of sample preparation and the longer residence time (Barbeau et al., 1981; Louchouarn and Lucotte, 1998; Santschi et al., 1999; Williams, Dellapenna, et al., 2015). For example, T-Hg Hg concentration profile has been use as a geochronology tool to determine sediment accumulation rate for specific regions where there is clear anthropogenic loading of Hg (Louchouarn and Lucotte, 1998). Barbeau et al. (1981) indicate that Hg can be used as a core dating method similar to ^{137}Cs isotopes in the Saguenay Fjord. For this study, similarities between independent dating techniques ^{137}Cs and Hg in core 22 (Figure 3.4) verifies that T-Hg profile in HSC could be used as a geochronological marker. However, this method of dating should not be used independently because it is different from region to region and also the point input sources, mixing and dredging activities could affect signal and maximum concentration depth of T-Hg in the sediments.

3.3.2 Biomarkers as evidence of environmental change

3.3.2.1 Evidence from organic matter isotopic signature

Several studies within coastal and estuarine systems have used stable isotopes as tracers for organic matter, to distinguish between allochthonous versus autochthonous sources, and also to determine the influence of anthropogenic activities (Bianchi and Canuel, 2011; Brandenberger et al., 2011; Louchouarn et al., 1999; Sánchez-García et al., 2009; Williams et al., 2014). Anthropogenic activities in Galveston Bay have resulted in a significant shift in stable isotopic signatures (Figures 3.3 and 3.4). The sedimentary record shows a clear shift between 1930-1950 for core 13 and in the early 1920s for core 22. The most notable trend in $\delta^{13}C$ values for core 22 is at 76 cm and 111 cm - the depths that have the highest T-Hg and Pb values. The depth of the most negative $\delta^{13}C$ value of -25.84‰ is about 110 cm. Furthermore, a value of -25.84‰ was found to be associated with the Pb peak in the sediment, which is within the range of the $\delta^{13}C$ values for petroleum average of -28‰ (Faure, 1986). On the other hand, the $\delta^{15}N$ values (Figures 3.3 and 3.4; Tables 3.2 and 3.3) show a shift at the same depth as the $\delta^{13}C$ values. However, as the systems shifted from a marine dominated system to more terrestrially dominated system, the $\delta^{15}N$ profile shows enrichment compared to typical values. Several studies indicate that the enrichment in the $\delta^{15}N$ values may be the result of a combination of heavy nitrogen loading from agricultural fertilizers and sewage wastes (Bianchi and Canuel, 2011; Brandenberger et al., 2011; Williams et al., 2014). Therefore, the enriched $\delta^{15}N$ values are interpreted as an indication of increased anthropogenic activities in these locations.

Moreover, a binary mixing model was used from the isotopic data given in Tables 3.2 and 3.3 to evaluate the contribution of terrigenous organic matter (TOM) input to further assess these changes. The terrestrial and marine end-member values have been chosen based on the maximum depleted value found in these locations (-25.84‰) and the most enriched value (-18.87‰) respectively. These values are within the published ranges for isotope values in estuaries (Bianchi and Canuel, 2011). The terrestrial contribution (%TOM) to total organic carbon in sediment is determined by the following equation (Louchouarn et al., 1999):

$$\frac{[\delta^{13}C]_S - [\delta^{13}C]_M}{[\delta^{13}C]_T - [\delta^{13}C]_M}$$

Where subscripts represent the sample (S), marine end-member (M), and terrestrial end-member (T). Based on these end-members, the proportion of TOM in the two locations during the last century ranged from 30- 90% (Tables 3.2 and 3.3). These calculations show that there is a significant increase in TOM as a result of anthropogenic activities in the region. The rapid increase in industrialization and urbanization in GB during the early 1900s along with restricted tidal exchange has increased the terrestrial signal in the system. This conclusion is based on just $\delta^{13}C$ and $\delta^{13}N$ values. Many published studies show that changing the environmental conditions may cause a shift in the isotopic end-member values (Louchouarn et al., 1999; Williams et al., 2014). Moreover, more C4 plants input to the systems (enriched in $\delta^{13}C$) could have altered the $\delta^{13}C$ values as well, since they have values within the range of the marine end-member (Bianchi, 2007). Therefore, in order to minimize the uncertainty in the $\delta^{13}C$ values, lignin phenols were analyzed to trace vascular plant input to the system.

Table 3.2 Elemental and molecular concentration and molecular intensive ratios of sediments for core 13 (Clear Lake) in GB. TOC, total organic carbon (mg mg^{-1}); $\delta^{13}C$ and $\delta^{15}N$, stable carbon and nitrogen isotopic composition of organic carbon (‰VPDB); Σ_8 mass normalized yields of the eight lignin derived phenolic oxidation products (mg g^{-1}); Λ_8, carbon normalized yields of the eight lignin derived phenolic oxidation products (mg 100mg-OC^{-1}); S/V: ratio of syringyl to vanillyl phenols; C/V: ratio of cinnamyl to vanillyl phenols; $(Ad/Al)_V$: ratio of vanillic acid to vanillin; %OM, terrigenous organic matter percentages. N.D. not determined.

Core	Depth interval (cm)	TOC	$\delta^{13}C$	$\delta^{15}N$	Σ_8	Λ_8	S/V	C/V	$(Ad/Al)_V$	%TOM
13	0.5	1.4	-23.50	9.22	0.21	1.81	1.384	0.357	0.35	66.4
	5.5	1.5	-23.63	8.05	0.16	1.41	1.291	0.320	0.30	68.3
	10.5	1.1	-23.67	8.65	0.15	1.34	1.335	0.348	0.33	68.8
	15.5	1.3	-23.63	8.48	0.16	1.36	1.325	0.337	0.31	68.3
	20.5	1.4	-23.29	8.09	0.14	1.19	1.323	0.337	0.31	63.4
	25.5	1.3	-23.48	9.02	0.16	1.38	1.307	0.319	0.30	66.2
	30.5	1.4	-23.21	8.08	0.19	1.74	1.083	0.255	0.26	62.2
	35.5	1.6	-23.00	8.19	0.11	0.93	1.275	0.313	0.31	59.3
	40.5	1.3	-22.89	7.95	0.11	0.98	1.369	0.330	0.32	57.7
	45.5	1.4	-23.08	7.93	0.14	1.27	1.372	0.339	0.32	60.3
	50.5	1.3	-22.98	9.21	0.15	1.18	1.404	0.405	0.33	58.9
	55.5	1.5	-22.26	8.41	0.10	0.82	1.332	0.366	0.31	48.6
	60.5	1.1	-21.18	7.25	0.08	0.96	1.549	0.452	0.39	33.1
	65.5	1.0	-21.25	7.64	0.07	0.74	1.434	0.337	0.30	34.1
	70.5	1.0	-22.13	6.45	0.12	1.43	1.352	0.311	0.28	46.8
	75.5	1.2	-21.22	7.19	0.06	0.59	1.437	0.334	0.34	33.7
	80.5	0.7	-22.11	5.51	0.13	1.66	1.303	0.306	0.30	46.4
	85.5	1.0	-20.99	6.59	0.13	1.66	1.368	0.360	0.26	30.4
	90.5	1.0	-19.84	5.14	0.07	0.87	1.903	0.311	0.32	14.0
	95.5	0.7	-19.83	2.89	0.05	0.79	1.444	0.245	0.33	13.8
	100.5	1.1	-19.19	1.86	0.07	0.85	1.609	0.257	0.31	4.6
	105.5	0.6	-18.90	1.56	0.06	1.04	1.871	0.236	0.30	0.4
	110.5	0.3	-19.03	4.69	0.05	2.33	1.983	0.243	0.31	2.2
	115.5	0.2	-18.87	4.16	0.03	1.88	1.476	0.195	0.42	0.1
	120.5	0.2	-18.91	2.86	0.03	1.76	1.894	0.249	0.35	0.5
	125.5	0.2	-19.08	3.12	0.03	1.42	1.816	0.188	0.27	3.1
	130.5	0.3	-19.28	2.41	0.04	2.52	1.422	0.128	0.23	5.9
	135.5	0.1	-18.90	5.58	0.02	2.31	1.619	0.231	0.32	0.5
	140.5	0.2	-18.90	2.62	0.03	1.60	1.756	0.273	0.32	0.4

Table 3.3 Elemental and molecular concentration and molecular intensive ratios of sediments for core 22 (HSC) in GB. TOC, total organic carbon (mg mg^{-1}); $\delta^{13}C$ and $\delta^{15}N$, stable carbon and nitrogen isotopic composition of organic carbon (‰VPDB); Σ_8 mass normalized yields of the eight lignin derived phenolic oxidation products (mg g^{-1}); Λ_8, carbon normalized yields of the eight lignin derived phenolic oxidation products (mg 100mg-OC^{-1}); S/V: ratio of syringyl to vanillyl phenols; C/V: ratio of cinnamyl to vanillyl phenols; $(Ad/Al)_V$: ratio of vanillic acid to vanillin; TOM, terrigenous organic matter percentages. N.D. not determined.

Core	Depth interval (cm)	TOC	$\delta^{13}C$	$\delta^{15}N$	Σ_8	Λ_8	S/V	C/V	$(Ad/Al)_V$	%TOM
22	0.5	1.1	-23.67	8.30	0.04	0.35	0.449	0.026	2.66	68.9
	5.5	1.3	-23.31	7.11	0.03	0.22	0.466	0.022	2.84	63.7
	11	0.8	-22.75	8.68	0.01	0.10	0.529	0.033	3.62	55.7
	15	0.9	-22.66	6.75	0.01	0.13	0.610	0.003	3.53	54.4
	21	1.0	-23.33	8.69	0.01	0.07	0.536	0.002	4.37	64.1
	25	1.0	-23.27	8.71	0.01	0.07	0.466	0.005	4.00	63.1
	31	1.4	-23.53	7.63	0.01	0.07	0.485	0.002	4.27	66.9
	35	1.1	-23.67	7.52	0.01	0.06	0.457	0.003	4.43	68.8
	41	1.2	-23.51	8.37	0.01	0.10	0.406	0.003	4.94	66.7
	45	1.0	-23.34	8.36	0.01	0.05	0.374	0.004	3.90	64.2
	51	1.5	-23.66	8.57	0.01	0.08	N.D.	0.033	3.15	68.8
	56	1.3	-23.70	6.38	0.02	0.18	0.440	0.037	3.34	69.3
	61	1.3	-23.58	6.23	0.02	0.17	0.493	0.036	3.66	67.5
	66	1.5	-23.39	5.57	0.03	0.26	0.580	0.035	3.30	64.9
	71	1.3	-23.56	5.02	0.04	0.34	0.504	0.071	3.32	67.3
	76	2.2	-25.25	2.40	0.04	0.25	0.362	0.021	3.11	91.5
	81	1.9	-24.89	2.47	0.03	0.16	0.579	0.038	2.44	86.3
	86	1.4	-23.81	4.06	0.03	0.19	0.580	0.029	2.72	71.0
	91	2.1	-24.28	3.96	0.03	0.19	0.516	0.039	3.03	77.6
	96	1.4	-22.70	5.01	0.02	0.21	0.618	0.068	2.91	54.9
	101	1.9	-24.37	5.64	0.02	0.15	0.569	0.037	2.65	79.0
	106	2.0	-23.88	6.61	0.02	0.11	0.591	0.040	2.47	71.9
	111	5.5	-25.84	4.93	0.02	0.04	0.523	0.065	2.47	100.0
	116	2.0	-24.82	5.23	0.03	0.15	0.800	0.050	2.47	85.5
	121	1.7	-21.55	3.45	0.04	0.22	0.650	0.046	2.83	38.4
	126	1.2	-20.94	3.05	0.03	0.21	0.743	0.088	2.38	29.8
	131	0.5	-20.60	1.55	0.01	0.22	0.676	0.072	2.17	24.9
	136	0.4	-20.45	2.81	0.01	0.18	0.735	0.053	2.26	22.7
	141	0.3	-20.63	0.50	0.01	0.37	0.760	0.076	2.23	25.2

3.3.2.2 Historical trend and signature of LOPs

Lignins are the second highest naturally abundant group of polymeric materials found in the cell wall of vascular plants (Burdige, 2006; Sarkanen and Ludwig, 1971). Due to this structural feature, the decomposition of lignin is relatively slow under both aerobic and anaerobic conditions. CuO oxidation of lignin phenols produces 11 phenolic monomers, which can be classified into four families; *p*-hydroxyl (P), vanillyl (V), syringyl (S), and cinnamyl (C). Furthermore, because vascular plants are confined to land, lignin represents an important tracer of terrestrial organic matter (Bianchi and Canuel, 2011; Hedges and Ertel, 1982; Hedges and Mann, 1979; Kuo et al., 2008). Lignin phenols were used to record shifts in sources of terrestrial organic matter (TOM) and reconstruct impacts of industrialization and urbanization in HSC and Clear Lake, respectively. Figures 3.3 and 3.4 show profiles of the sum of eight lignin oxidation products (LOPs) as the sum of eight oxidation products phenols (Σ8) and the state of oxidative degradation of lignin constituents (the ratio of acid to aldehyde phenols (Ad/Al) of vanillyl phenol) was used to determine the environmental shift in the load of organic matter input to Galveston Bay during the last century. The lignin profiles (Figures 3.3 and 3.4) show a significant increase in both cores, starting from the early 1900s and show a historical peak in the 1960s-1970s in core 22. Furthermore, a similar trend was observed with the carbon-normalized yields of the eight lignin-derived phenols (Λ8) in Galveston Bay (Tables 3.2 and 3.3). The lignin profile and timing is consistent with the anthropogenic activities in the region and comparable with other regions in the world (Brandenberger et al., 2008; Brandenberger et al., 2011; Kuo et al.,

2014). Lignin and trace metal profiles confirm that increased industrialization, urbanization, and land clearing has led to greater inputs of TOM to the aquatic system of Galveston Bay. In both locations, the concentration of lignin is still increasing which reflect that there is still TOM input from the system. Moreover, another explanation for the higher concentration near the surface sediment in core 22 locations is the continuing erosion of organic-rich material from the waste pits around 2012 (EPA, 2015). Furthermore, tropical storms could enhance TOM inputs to the system by soil erosion and sediment transport from land and the waste pits (Kuo et al., 2014). Although there is an increase in lignin input to the surface sediment, this increase does not mean that the environmental regulations on both the pulp and paper mills industry following the lignin peak are not effective. On the other hand, the Σ8 peak at depth 120 cm (1930s) is occurring around the beginning of the last century. Moreover, the fluctuations in the lignin profiles reflect the production fluctuations in the pulp and paper mills (Louchouarn et al., 1999). It is predicted that the inputs of TOM will continue to increase due to rapid increase in industrialization and urbanization in Galveston Bay compared to the reduction in trace metals input.

The yields and ratios of these lignin phenols provide information about the structure of vascular plants that may distinguish the group of vascular plant (angiosperm and gymnosperm) and tissue type (woody and non-woody). The ratio of syringyl (S) and cinnamyl (C) to vanillyl (V) phenols was used to further evaluate the sources of the TOM inputs to Galveston Bay. Syringyl structural units are unique in angiospermous lignin and absent from gymnospermous tissues, while cinnamyl groups are common to

angiosperms and non-gymnosperms and absent from woody gymnospermous (Bianchi and Canuel, 2011; Goni and Hedges, 1992; Hedges and Ertel, 1982; Hedges and Mann, 1979; Louchouarn et al., 2000). Figure 3.7 shows that different types of primary TOM lignin source dominate the two cores. Core 22 shows that the woody gymnosperm is the primary source. Several studies indicate that paper mill industries prefer softwood (gymnosperm) than hardwood (angiosperm) in North America, which altered the sedimentary lignin signature during the last century (Brandenberger et al., 2011; Louchouarn et al., 1999). The strong drop in C/V signature below the surface sediment is associated with a significant decrease in lignin inputs and sediment digenesis (Figures 3.4 and 3.7; Table 3.3). On the other hand, core 13 shows that non-woody angiosperm leaves and grasses are the primarily sources of TOM.

The degree of oxidative degradation of lignin constituents was determined by the ratio of vanillic acid to vanillin $(Ad/Al)_{V,}$ which is due to microbial, photochemical, and degradation processes (Bianchi and Canuel, 2011; Louchouarn et al., 1999). The $(Ad/Al)_V$ values (Figures 3.3 and 3.4) show a narrow range (0.27-0.42) for core 13 and a wider range (2.17-4.94) for core 22. These $(Ad/Al)_V$ values for core 13 suggest the freshness of the lignin material inputs to the system (Kuo et al., 2014). The wider range in core 22 could be explained that the woody material had experienced extensive degradation alteration. Studies show that industrial pulping and decomposition within contaminated sediments is known to oxidatively alter the lignin signature and have a higher $(Ad/Al)_V$ ratio (Louchouarn et al., 1999).

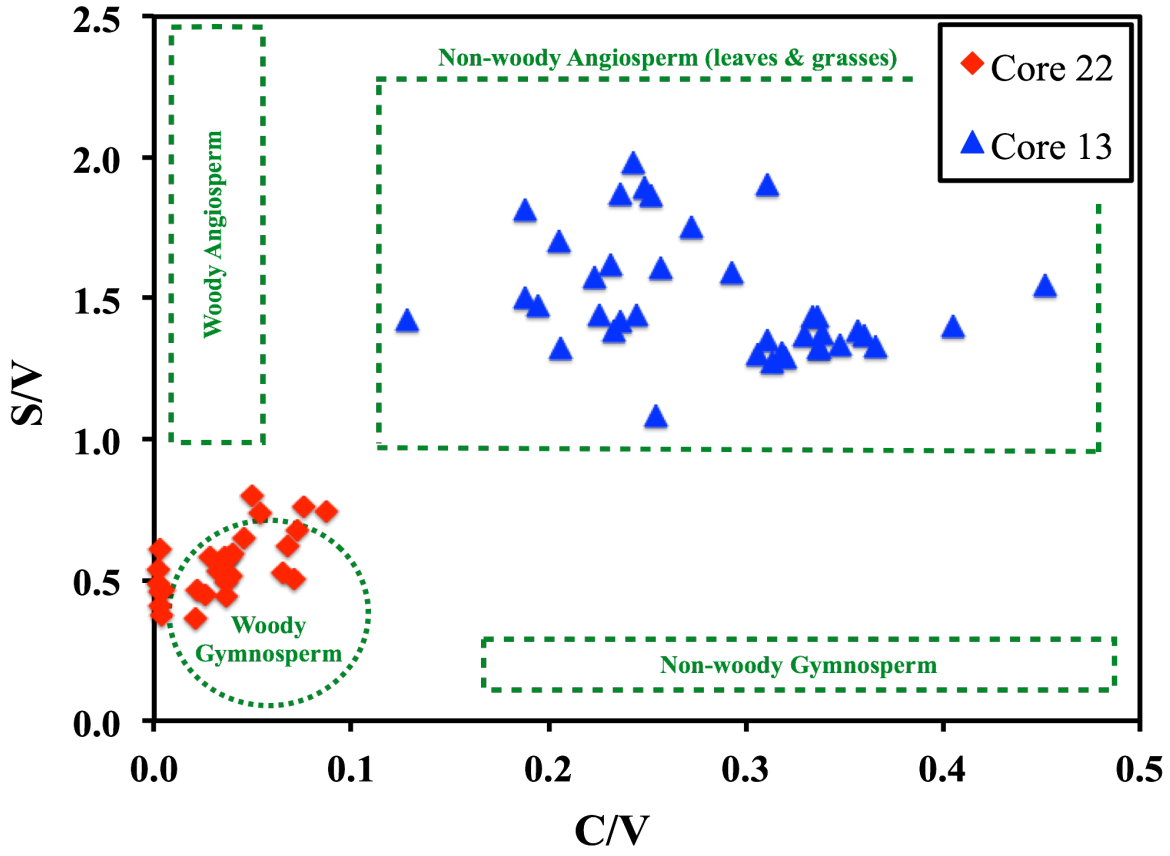

Figure 3.7 S/V *vs.* C/V plot for sediments from core 22 and core 13

3.3.3 Influence of environmental policies on contamination

3.3.3.1 Geoaccumulation index and enrichment factor

Between the 1960 and 1970, the HSC experienced massive fish kills, and the EPA identified the region as one of the most polluted aquatic systems in the United States (EPA, 1980; Lester and Gonzalez, 2011). Since then, several federal agencies have worked to implement the Clean Water Act (1972) in Galveston Bay to minimize the point sources of pollution (Lester and Gonzalez, 2011). Therefore, in order to assess the effectivnes of these environmental regulations on industrial point sources of contaminants and watershed land management, the geoaccumulation index and enrichment factor (EF) where calculated since the contaminated period (Table 3.4). The enrichment factor was calculated as the ratio of surface and maximum T-Hg to background concentrations. The geoaccumulation index (Müller, 1979) was used to assess the degree of contamination of Hg in the Bay using the following equation:

$$I_{geo} = \log_2(C_{Hg}/1.5B_{Hg})$$

Where I_{geo} is the geoaccumulation index, C_{Hg} is the concentration in the sediments, and B_{Hg} is the background concentration. The constant 1.5 is introduced to minimize the variation of background value due to lithogenetic variation. The I_{geo} calculated values were used to classify the sediment in terms of quality. The I_{geo} includes seven classes; (>5) (extremely polluted), strongly to extremely polluted (4-5), strongly polluted (3-4), moderately to strongly polluted (2-3), moderately polluted (1-2), unpolluted to moderately polluted (0-1), and unpolluted (<0), with the highest grade (>5) reflecting a 100-fold enrichment above the background values.

The I_{geo} and EF in Table 3.4 show that the system has improved in sediment quality over a period of 41 years due to the Clean Water Act that required all industries to upgrade their wastewater treatment facilities discharging to Galveston Bay (Lester and Gonzalez, 2011). Cores in HSC show a notable improvement where the I_{geo} shifts two to three classes lower than the more polluted period. For example core 22 showed an EF of 296.8 and I_{geo} class 6 in between 1960s and 1970s. Currently, the EF and I_{geo} has values of 20.3 and class 4, respectively. Although the system (HSC) has improved, it is still considered strongly polluted. As mentioned earlier, the EPA stated a section of the HSC as a Superfund Site on the National Priority List and designated some areas of concern (EPA, 2015). However, core 22, where there is high Hg concentration and other trace metals is not included among the area of concern (Figure 3.8). Therefore, it is recommended to expand the area of concern to include Scott Bay and other possible surrounding sub-bays. Similarly, the Clear Lake region has shown an improvement, but at a lower rate. These results clearly distinguish between the effect of industrialization and urbanization to the quality of the aquatic systems. The point sources were eliminated following the Clean Water Act; however, non-point sources from residential, industrial, agricultural lands, and dredging activities still need to be addressed. Determining a recovery rate back to pre-industrial levels is a valuable gauge on the recovery of the system since the sediment quality is improving.

Table 3.4 Degree of contamination based on (Müller) geoaccumulation index (I_{geo} Class), which used to assess the sediment quality classification. [a]Represents the contamination period between 1960s and 1970s. [b]Enrichment factor determined as ratio of surface and maximum to background concentrations.

Region	Core	Maximum[a]		Surface	
		I_{geo} Class	E.F.[b]	I_{geo} Class	E.F.[b]
Clear Lake	12	3	6.3	2	4.5
	13	4	10.2	3	7.8
Taylor Lake	14	2	3.3	1	2.5
	15	3	11.0	3	8.2
	16	3	7.1	2	4.9
	17	2	5.3	2	3.0
HSC	18	3	11.6	1	2.2
	19	4	12.1	0	0.9
	20	4	15.8	1	2.0
	21	6	93.8	1	2.1
	22	6	296.8	4	20.3

Figure 3.8 San Jacinto paper mill disposal waste pits (red) and Area of concern (orange) by Environmental Protection Agency (EPA), Texas Commission on Environmental Quality (TCEQ), and US Army Corps of Engineers (USACE) (EPA, 2015) with core 22 in Scott Bay.

3.3.3.2 Rates of recovery.

The recovery rate was calculated from the maximum T-Hg inputs in core 22 and core 13 using a linear regression approach method (Figure 3.9) (Brandenberger et al., 2008; Louchouarn et al., 2012). The recovery rate is calculated based on several assumptions: (1) no major increase in the watershed developments, (2) constant sediment supply and mixing, and (3) all current Hg sources were to stop or reduced significantly. The first assumption might not be true in the case of Galveston Bay since the bay is expected to expand in population, which shifts the contaminant sources from point source to more complex non-point sources, making our estimations minimum recovery times. The regression analyses indicate a significant ($p > 0.01$) break in the linearity occurring around the 1990s in core 13 and 1982 in core 22. These analyses indicate that the recovery rate has reduced (non-linear trends) separate recovery rate for the twenty-first century. The recovery rate for the 20th century was predicted to reach background concentration by 2069 ± 11 for core 13 and 2012 ± 1 for core 22. The faster recovery rate for core 22 is due to the faster sediment accumulation rate and the significant reduction in point sources of Hg in the region. The lower sediment accumulation rate and the lower Hg input compared to core 22 could explain the longer recovery time (Table 3.1). On the other hand, the twenty-first century has a longer recovery rate due to the increase in urbanization and the influence of the non-point source inputs to the system. The system is estimated to recover by 2115 ± 35 and 2044 ± 8 for core 13 and 22, respectively. These results suggest that the non-point sources (diffuse) may impede the continued progress in recovery (Brandenberger et al., 2008).

More study is needed to determine the new emission sources of Hg and other trace metals in the system and also the possible emission from the legacy contamination from dredging activities, and the increase in the non-point inputs to the system.

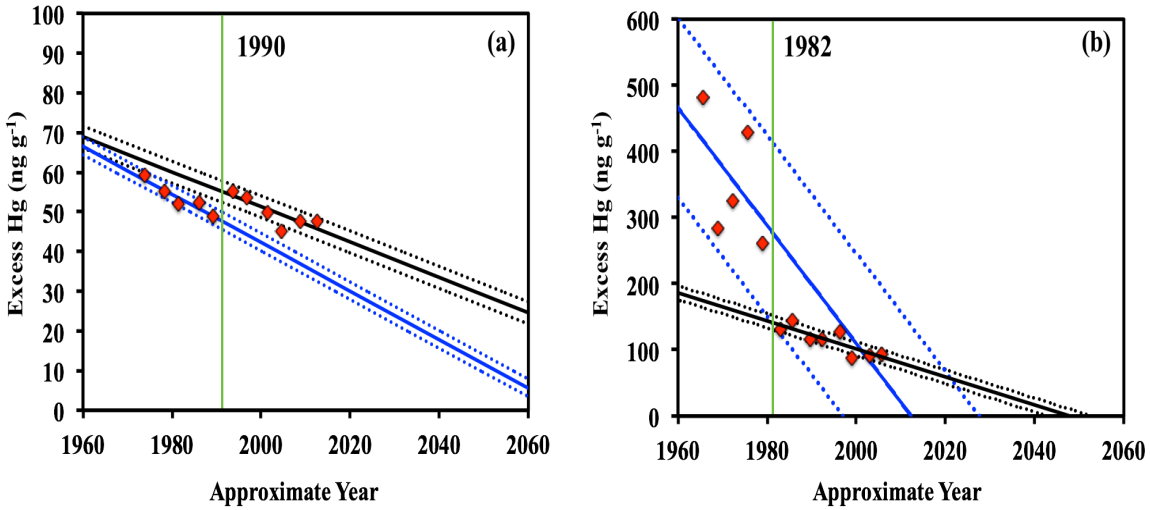

Figure 3.9 Estimated natural recovery rates for the 20th and twenty-first century for both core 13 (a) and core 22 (b) determined from linear regression of the excess metal concentration after the Hg peak in 1960s-1970s. The regressions and 95% confidence intervals are shown for the 20th centaury (Blue) and for the twenty-first century (Black) for the excess Hg concentration. The green line represents the linearity breaks.

3.4 Conclusions

Sediment cores collected in Galveston Bay provide a historical record of trace metal contaminantion and discharges over the last century. T-Hg inputs in the bay had significantly increased and show enrichments in deeper sediments during the 1960s-1970s, and reductions towards the sediment surface. Other trace metals also show a similar trend to T-Hg, with noted exception of Pb, which showed enrichments deeper in the HSC sediment column. The results show that industrialization in HSC, especially the Chlor-Alkali plant, is the major source of T-Hg to the aquatic system, including with atmospheric inputs from industrial sources. Surficial Hg concentrations were found to be significantly higher proximal to the SJR/HSC, and decrease seaward and within the back barrier lagoons. This study demonstrates the ability of using Hg as a corroborating geochronological tool, and that its use may support the validity of the other traditional methods used in estuaries. The upper portion of the bay thus acts as a filter that traps the contaminants within the estuarine sediments, lowering the amount discharged to the sea. It is important to consider the biological production of the bay and the chemical cycles of contaminants in the sediment and the water column. Therefore, it is essential not to disturb the sediment column. X-radiographs and ^{210}Pb profiles show that bioturbation and physical sediment mixing is minimal in the most contaminated areas. Consequently, disturbing the sediment column will have a significant potential to reintroduce higher concentrations of legacy contaminants. As such, we recommend against dredging in areas where there are high concentrations of legacy contaminants at depth.

Along with the significant shift in the inputs of trace metals in the system, stable isotopes and lignin show a dramatic shifts and an increase of the TOM input through the Anthropocene. Lignin diagenetic signature $(Ad/Al)_v$ in core 22 were high, which indicate that woody materials experience extensive alteration due to the paper pulp activities and the potential input from the paper pulps waste pits. On the other hand, the $(Ad/Al)_v$ ratio in Clear Lake (Core 13) indicates the freshness of the material deposited in the system. Moreover, Core 22 shows that woody gymnosperm is the primary source and core 13 shows that the non-woody angiosperm leaves and grasses are the primary sources. The different sources reflect the different influence of industrialization and urbanization to the aquatic system. Finally, the twenty-first century seems to have a lower recovery rate toward a pre-industrial concentration due to the removal of point sources. A new approach is needed to regulate the non-point sources that will continue to increase in Galveston Bay and other developed bay around the world in order to achieve healthier ecological systems.

CHAPTER IV

CONCLUSIONS

In the studies presented here, we have investigated the influence of anthropogenic activities on the aquatic system in Galveston Bay. The first study focused on the elevated land subsidence due to groundwater withdrawal on the bay and how land subsidence impacts sediment accumulation rate. The second study investigated the impact of the anthropogenic alterations on the fate and transport of the historical inputs of mercury and other contaminants and how the economic development of the region has increased the input of mercury within the last 100 years. The results of the two studies are summarized as follows:

- Sedimentation rates in Galveston Bay did not keep pace with elevated formation of accommodation space. Due to the development of hydrocarbon refineries around Galveston Bay (including the Houston Ship Channel) there has been elevated subsidence beginning around 1900. There is a gradient going down the bay, with lower subsidence generally towards the south and east. Moreover, the sediment accumulation rate shows a similar gradient; however, at a lower rate. The final results show that sediment accumulation rates are 50% lower than the Relative Sea Level Rise (RSLR), and therefore, Galveston Bay is experiencing a sediment deficit. Groundwater withdrawal in the bay, dredging activities and the

reduction of river discharges (due to dam building) have vastly impacted sedimentary transport and accumulation.

- During the last century, anthropogenic activities in Galveston Bay have caused a shift in trace metal and biomarker signals within the sediment record. Results reveal an extremely high concentration of Hg at 50-80 cm of depth in the Houston Ship Channel. This layer poses a risk for in increased Hg loading if exposed and re-mobilized within the bay, ultimately threatening the health of the ecosystem. This study shows a gradient in Hg concentration being high in Houston Ship Channel and decrease toward the open water. Historical reconstructions of sediment cores indicate an increase in Hg above background values beginning between the 1960s-1970s. Chlor-Alkali is the primary anthropogenic sources of Hg in the bay, which correspondingly increased at this time. These results suggest the utility of using Hg as a regional geochronological tool, provided that source inputs are similar. Furthermore, anthropogenic activities have altered the depositional environment and organic signatures ($\delta^{13}C$ and lignin). Biomarker results show an increase in Terrigenous Organic Matter (TOM) inputs during the last century. Finally, contaminant levels and recovery rates indicate that the system is slowly improving toward pre-industrialization conditions, reflecting increased environmental regulations over the last several decades. However, in the next century it is expected that non-point sources of contaminants will increase with further population growth and land reclamation.

Further investigation is required to assess the role of different processes at the sediment-water interface on the contamination cycle in the water column to develop better management strategies in estuaries globally.

REFERENCES

Acquavita, A., Covelli, S., Emili, A., Berto, D., Faganeli, J., Giani, M., Horvat, M., Koron, N., Rampazzo, F., 2012. Mercury in the sediments of the Marano and Grado Lagoon (northern Adriatic Sea): Sources, distribution and speciation. Estuarine Coastal and Shelf Science 113, 20-31.

Al-Mukaimi, M., 2016. Sediment accumulation rate and relative sea level rise in Galveston Bay, Department of Oceanography. Texas A&M University, College Station, thesis

AMAP/UNEP, 2008. Technical Background Report to the Global Atmospheric Mercury Assessment. Arctic Monitoring and Assessment Program. UNEP Chemicals Branch, 159 p.

Anderson, J.B., 2007. The formation of the Upper Texas Coasts; A Geological Answers Questions about Sand, Storms & Living by the Sea Texas A&M University Press, College Station, USA.

Anderson, J.B., 2011. Chapter 5-Physical Form and Processes, in: Lester, L.J., Gonzalez, L.A. (Eds.), The State of the Bay: A Characterization of the Galveston Bay Ecosystem, third ed. Texas Commission on Environmental Quality, Galveston Bay Estuary Program, Houston, USA, p. 21.

Balogh, S.J., Engstrom, D.R., Almendinger, J.E., Meyer, M.L., Johnson, D.K., 1999. History of mercury loading in the Upper Mississippi River reconstructed from the sediments of Lake Pepin. Environmental Science & Technology 33, 3297-3302.

Bank, M.S., 2012. Mercury in the Environment: Pattern and Process. University of California Press, Berkely and Los Angeles, California.

Barbeau, C., Bougie, R., Cote, J.E., 1981. Temporal and Spatial Variations of Mercury, Lead, Zinc, and Copper in Sediments of the Saguenay Fjord. Canadian Journal of Earth Sciences 18, 1065-1074.

Barusseau, J.P., Ba, M., Descamps, C., Diop, E.S., Diouf, B., Kane, A., Saos, J.L., Soumare, A., 1998. Morphological and sedimentological changes in the Senegal River estuary after the constuction of the Diama dam. Journal of African Earth Sciences 26, 317-326.

Bawden, G.W., Johnson, M.R., Kasmarek, M.C., Brandt, J., Middleton, C.S., 2012. Investigation of land subsidence in the Houston-Galveston region of Texas by using the Global Positioning System and interferometric synthetic aperture radar. 1993–2000: U.S. Geological Survey Scientific Investigations Report 2012–5211, 88.

Bianchi, T.S., 2007. Biogeochemistry of Estuaries. Oxford University Press, Oxford; New York.

Bianchi, T.S., Canuel, E.A., 2011. Chemical Biomarkers In Aquatic Ecosystems. Princeton University Press, Princeton.

Blum, M.D., Sivers, A.E., Zayac, T., Goble, R.J., 2003. Middle Holocene Sea-Level and Evolution of the Gulf of Mexico Coast. GCAGS/GCSSEPM Transactions 53, 64-77.

Brandenberger, J.M., Crecelius, E.A., Louchouarn, P., 2008. Historical inputs and natural recovery rates for heavy metals and organic biomarkers in Puget Sound during the 20th century. Environ Sci Technol 42, 6786-6790.

Brandenberger, J.M., Louchouarn, P., Crecelius, E.A., 2011. Natural and Post-Urbanization Signatures of Hypoxia in Two Basins of Puget Sound: Historical Reconstruction of Redox Sensitive Metals and Organic Matter Inputs. Aquatic Geochemistry 17, 645-670.

Burdige, D.J., 2006. Geochemistry of Marine Sediments. Princeton University Press, New Jersey.

Byun, D.S., Wang, X.H., Holloway, P.E., 2004. Tidal characteristic adjustment due to dyke and seawall construction in the Mokpo Coastal Zone, Korea. Estuarine, Coastal and Shelf Science 59, 185-196.

Carbognin, L., Teatini, P., Tosi, L., 2004. Eustacy and land subsidence in the Venice Lagoon at the beginning of the new millennium. Journal of Marine Systems 51, 345-353

Choi, M., Park, J., Cho, D., Jang, D., Kim, M., Choi, J., 2015. Tracing metal sources in core sediments of the artificial lake An-Dong, Korea: Concentration and metal association. Science of The Total Environment 527-528, 384-392.

Church, J.A., P.U. Clark, A. Cazenave, J.M. Gregory, S. Jevrejeva, A. Levermann, M.A. Merrifield, G.A. Milne, R.S. Nerem, P.D. Nunn, A.J. Payne, W.T. Pfeffer, Stammer, D., Unnikrishnan, A.S., 2013. Sea Level Change, in: Stocker, T.F., D. Qin, G.-K. Plattner, M. Tignor, S.K. Allen, J. Boschung, A. Nauels, Y. Xia, Bex, V., Midgley, P.M. (Eds.), Climate Change 2013: The Physical Science Basis. Contribution of Working Group I to the Fifth Assessment Report of the Intergovernmental Panel on Climate Change. Cambridge University Press, New York, USA.

Clark, S., Bornschein, R., Succop, P., Roda, S., Peace, B., 1991. Urban Lead Exposures of Children in Cincinnati, Ohio. Chemical Speciation and Bioavailability, Vol 3, Nos 3-4, December 1991, 163-171.

Coplin, L.S., Galloway, D., 1999. Houston-Galveston, Texas Managing coastal subsidence, in: Galloway, D., Jones, D.R., Ingebritsen, S.E. (Eds.), Land subsidence in the United States. U.S. Geological Survey Circular 1182, pp. 35-48.

Day, J.W., Rybczyk, J., Scarton, F., Rismondo, A., Are, D., Cecconi, G., 1999. Soil accretionary dynamics, sea-level rise and the survival of wetlands in Venice Lagoon: A field and modelling approach. Estuarine Coastal and Shelf Science 49, 607-628.

Day, J.W., Yanez-Arancibia, A., Kemp, W.M., 2013. Human Impact and Management of Coastal and Estuarine Ecosystems, in: Day, J.W., Crump, B.C., Kemp, W.M., Yanez-Arancibia, A. (Eds.), Esturine Ecology, 2 ed. John Wiley and sons, New Jersey, USA.

Dellapenna, T.M., Allison, M.A., Gill, G.A., Lehman, R.D., Warnken, K.W., 2006. The impact of shrimp trawling and associated sediment resuspension in mud dominated, shallow estuaries. Estuarine Coastal and Shelf Science 69, 519-530.

Dellapenna, T.M., Kuehl, S.A., Schaffner, L.C., 1998. Sea-bed mixing and particle residence times in biologically and physically dominated estuarine systems: a comparison of lower Chesapeake Bay and the York River subestuary. Estuarine Coastal and Shelf Science 46, 777-795.

Dellapenna, T.M., Kuehl, S.A., Schaffner, L.C., 2003. Ephemeral deposition, seabed mixing and fine-scale strata formation in the York River estuary, Chesapeake Bay. Estuarine, Coastal and Shelf Science 58, 621-643.

Di Leonardo, R., Tranchida, G., Bellanca, A., Neri, R., Angelone, M., Mazzola, S., 2006. Mercury levels in sediments of central Mediterranean Sea: a 150+ year record from box-cores recovered in the Strait of Sicily. Chemosphere 65, 2366-2376.

Donnelly, J.P., Bertness, M.D., 2001. Rapid shoreward encroachment of salt marsh cordgrass in response to accelerated sea-level rise. Proc Natl Acad Sci U S A 98, 14218-14223.

Eggleston, J., Pope, J., 2013. Land subsidence and relative sea-level rise in the southern Chesapeake Bay region U.S. Geological Survey Circular 1392, 30 p.

EPA, 1980. A water quality success story: Lower Houston Ship Channel and Galveston Bay, Texas. Washington, DC: US Environmental Protection Agency, Office of Water Planning and Standards.

EPA, 1998. Method 7473: Mercury in Solids and Solutions by Thermal Decomposition Amalgamation and Atomic Absorption Spectrophotometry, EPA SW-846. USEPA Office of Research and Development Environmental Monitoring Systems Labratory, Cincinnati.

EPA, 2007. National Estuary program coastal condition report, Chapter: Gulf of Mexico National Estuary Program Coastal Condition. , Galveston Bay Estuary Program.

EPA, 2015. EPA Superfund Program: San Jacento River Waste Pits, Channelview, TX. Available at http://cumulis.epa.gov/supercpad/cursites/csitinfo.cfm?id=0606611.

Faure, G., 1986. Principles of Isotope Geology, 2 ed. John Wiley & Sons, New York, USA.

Feagin, R.A., Sherman, D.J., Grant, W.E., 2005. Coastal erosion, global sea-level rise, and the loss of sand dune plant habitats. Frontiers in Ecology and the Environment 3, 359-364.

Gao, J.-H., Li, J., Wang, H., Bai, F.-l., Cheng, Y., Wang, Y.-p., 2012a. Rapid changes of sediment dynamic processes in Yalu River Estuary under anthropogenic impacts. International Journal of Sediment Research 27, 37-49.

Gao, J.H., Li, J., Wang, H., Bai, F.L., Cheng, Y., Wang, Y.P., 2012b. Rapid changes of sediment dynamic processes in Yalu River Estuary under anthropogenic impacts. International Journal of Sediment Research 27, 37-49.

GBNEP, 1994. The state of the bay: a characterization of the Galveston Bay ecosystem. Galveston Bay National Estuary Program Publication 44.

GBST, 2016. Water and Sediment Quality Data Portal. Galveston Bay Status and Trends. Available at http://www.galvbaydata.org/WaterSediment/WaterandSedimentQuality/DataPortal/tabid/214/Default.aspx.

Goni, M.A., Hedges, J.I., 1992. Lignin Dimers - Structures, Distribution, and Potential Geochemical Applications. Geochimica et Cosmochimica Acta 56, 4025-4043.

Greene, C.E., 2016. CLEAR LAKE CITY, TX, Handbook of Texas. Texas State Historical Association, Available at http://www.tshaonline.org/handbook/online/articles/hjc23.

Han, S.H., Gill, G.A., Lehman, R.D., Choe, K.Y., 2006. Complexation of mercury by dissolved organic matter in surface waters of Galveston Bay, Texas. Marine Chemistry 98, 156-166.

Harmon, M., A. S. Pait, Hameedi, M.J., 2003. Sediment Contamination, Toxicity, and Macroinvertebrate Infaunal Community in Galveston Bay. NOAA Tech. Memo. NOS NCCOS CCMA 122. Silver Spring, MD: NOAA, NOS, Center for Coastal Monitoring and Assessment.

Healy, M.G., Hickey, K.R., 2002. Historic land reclamation in the intertidal wetlands of the Shannon estuary, western Ireland. Journal of Coastal Research, 365-373.

Hedges, J.I., Ertel, J.R., 1982. Characterization of Lignin by Gas Capillary Chromatography of Cupric Oxide Oxidation-Products. Analytical Chemistry 54, 174-178.

Hedges, J.I., Mann, D.C., 1979. Characterization of Plant-Tissues by Their Lignin Oxidation-Products. Geochimica et Cosmochimica Acta 43, 1803-1807.

HGSD, 2008. Houston Galveston Subsidence District- Subsidence: 1906–2000. Available at http://www.subsidence.org/Assets/PDFDocuments/.

HGSD, 2013. Subsidence and groundwater regulation FAQ's. Available at http://hgsubsidence.org/frequently-asked-questions/subsidence-groundwater-regulation-faqs/.

IPCC, 2007. Climate Change 2007: Impacts, Adaptation and Vulnerability, in: M.L. Parry, O.F. Canziani, J.P. Palutikof, Linden, P.J.v.d., Hanson, C.E. (Eds.), Contribution of Working Group II to the Fourth Assessment Report of the Intergovernmental Panel on Climate Change. Cambridge University Press, Cambridge, UK, p. 976 pp.

IPCC, 2013. Summary for Policymakers, in: Stocker, T.F., D. Qin, G.-K. Plattner, M. Tignor, S.K. Allen, J. Boschung, A. Nauels, Y. Xia, Bex, V., Midgley, P.M. (Eds.), Climate Change 2013: The Physical Science Basis. Contribution of Working Group I to the Fifth Assessment Report of the Intergovernmental Panel on Climate Change. Cambridge University Press, Cambridge, United Kingdom and New York, NY, USA.

Jelgersma, S., 1996. Land subsidence in Coastal lowlands, in: Milliman, J.D., Haq, B.U. (Eds.), Sea-Level Rise and Coastal Subsidence. Causes, Consequences, and Strategies. Kluwer Academic publisher, Netherland.

Kasmarek, M.C., Johnson, M.R., Ramage, J.K., 2012. Water-level altitudes 2012 and water-level changes in the Chicot, Evangeline, and Jasper aquifers and compaction 1973–2011 in the Chicot and Evangeline aquifers, Houston–Galveston region, Texas. U.S. Geological Survey Scientific Investigations Map 3230, 18 p., 16 sheets.

Kennish, M.J., 2002. Environmental threats and environmental future of estuaries. Environmental Conservation 29, 78-107.

Kennish, M.J., Paerl, H.W., 2010. Costal Lagoons, Critical Habitats of Environmental Change. CRC press, New York, USA.

Kolak, J.J., Long, D.T., Beals, T.M., Eisenreich, S.J., Swackhamer, D.L., 1998. Anthropogenic inventories and historical and present accumulation rates of copper in Great Lakes sediments. Applied Geochemistry 13, 59-75.

Kolker, A.S., Allison, M.A., Hameed, S., 2011. An evaluation of subsidence rates and sea-level variability in the northern Gulf of Mexico. Geophysical Research Letters 38.

Kuo, L.J., Lee, C.L., Louchouarn, P., Huh, C.A., Liu, J.T., Chen, J.C., Lee, K.J., 2014. A centennial record of anthropogenic impacts and extreme weather events in southwestern Taiwan: evidence from sedimentary molecular markers in coastal margin. Mar Pollut Bull 86, 244-253.

Kuo, L.J., Louchouarn, P., Herbert, B.E., 2008. Fate of CuO-derived lignin oxidation products during plant combustion: application to the evaluation of char inputs to soil organic matter. Organic Geochemistry 39, 1522-1536.

Lambeck, K., Chappell, J., 2001. Sea level change through the last glacial cycle. Science 292, 679-686.

Lan, X., Talbot, R., Laine, P., Torres, A., Lefer, B., Flynn, J., 2015. Atmospheric Mercury in the Barnett Shale Area, Texas: Implications for Emissions from Oil and Gas Processing. Environ Sci Technol 49, 10692-10700.

Laverty, P., 2014. Topographic and Base-level Control on Back-Barrier Lagoon Evolution: West Galveston Bay, TX, Department of Oceanography. Texas A&M University, thesis

Lester, J., Gonzalez, L., 2002. The State of the Bay, A Characterization of the Galveston Bay Ecosystem. The Galveston Bay Estuary Program (GBEP T-7).

Lester, J., Gonzalez, L., 2011. The State of the Bay: A Characterization of the Galveston Bay Ecosystem. Texas Commission on Environmental Quality, Galveston Bay Estuary Program, Houston, Texas, Third Edition Third Edition.

Liu, G., Cai, Y., O'Driscoll, N., 2012. Environmental chemistry and toxicology of mercury John Wiley & Sons, Inc, USA.

Long, E.R., 2000. Degraded Sediment Quality in U.S. Estuaries: A Review of Magnitude and Ecological Implications. Ecological Applications 10, 338-349.

Louchouarn, P., Kuo, L.J., Brandenberger, J.M., Marcantonio, F., Garland, C., Gill, G.A., Cullinan, V., 2012. Pyrogenic inputs of anthropogenic Pb and Hg to sediments of the Hood Canal, Washington, in the 20th century: source evidence from stable Pb isotopes and PAH signatures. Environ Sci Technol 46, 5772-5781.

Louchouarn, P., Lucotte, M., 1998. A historical reconstruction of organic and inorganic contamination events in the Saguenay Fjord St. Lawrence system from preindustrial times to the present. Science of The Total Environment 213, 139-150.

Louchouarn, P., Lucotte, M., Farella, N., 1999. Historical and Geographical Variations of Sources and Transport of Terrigenous Organic Matter within a Large-scale Coastal Environment. Organic Geochemistry 30, 675-699.

Louchouarn, P., Naehr, T.H., Silliman, J., Houel, S., 2006. Elemental, Stable Isotopic (13C), and Molecular Signatures of Organic Matter in Late Pleistocene-Holocene Sediments from the Peruvian Margin (ODP Site 1229). Proceedings of the Ocean Drilling Program, Scientific Results 201.

Louchouarn, P., S. Opsahl., Benner, R., 2000. Isolation and quantification of dissolved lignin from natural waters using solid-phase extraction (SPE) and GC/MS selected ion monitoring (SIM). Analytical Chemistry 13, 2780-2787.

McGranahan, G., Balk, D., Anderson, B., 2007. The rising tide: assessing the risks of climate change and human settlements in low elevation coastal zones. Environment and Urbanization 19, 17-37.

McLusky, D.S., Bryant, D.M., Elliott, M., 1992. The impact of land-claim on macrobenthos, fish and shorebirds on the forth estuary, eastern Scotland. Aquatic Conservation: Marine and Freshwater Ecosystems 2, 211-222.

Mitchell, S.B., Uncles, R.J., 2013. Estuarine sediments in macrotidal estuaries: Future research requirements and management challenges. Ocean & Coastal Management 79, 97-100.

Morris, J.T., Sundareshwar, P.V., Nietch, C.T., Kjerfve, B., Cahoon, D.R., 2002. Response of coastal wetlands to rising sea-levels. 38, 2869-2877.

Morse, J.W., B. J. Presley., Taylor, R.J., 1993. Trace Metal Chemistry of Galveston Bay: Water, Sediment and Biota. Marine Environmental Research 36, 1-37.

Müller, G., 1979. Schwermetalle in den sediments des Rheins-Veran-derungen seitt 1971. Umschau 79, 778-783.

Nichols, M.M., 1989. Sediment accumulation rate and relative sea level rise in lagoons, in: Ward, L.G., Ashley, G.M. (Eds.), Physical processes and sedimentology of siliciclastic dominated lagoonal systems. Marine Geology pp. 201-219.

Nitsche, F.O., Kenna, T.C., Haberman, M., 2010. Quantifying 20th century deposition in complex estuarine environment: An example from the Hudson River. Estuarine Coastal and Shelf Science 89, 163-174.

Nittrouer, C.A., DeMaster, D.J., McKee, B.A., Cutshall, N.H., Larsen, I.L., 1984. The effect of sediment mixing on Pb-210 accumulation rates for the Washington continental shelf. Marine Geology 54, 201-221.

Nittrouer, C.A., Sternberg, R.W., Carpenter, R., Bennett, J.T., 1979. The use of Pb-210 geochronology as a sedimentological tool: Application to the Washington continental shelf. Marine Geology 31, 297-316.

NOAA, 2013. Mean Sea Level Trend 8771450 Galveston Pier 21, Texas. Center for Operational Oceanographic Products and Services. Available at http://tidesandcurrents.noaa.gov/sltrends/sltrends_station.shtml?stnid=8771450.

Nutalaya, P., Yong, R.N., Chumnankit, T., Buapeng, S., 1996. Land subsidence in Bangkok during 1978-1988, in: Milliman, J.D., Haq, B.U. (Eds.), Sea-Level Rise and Coastal Subsidence. Causes, Consequences, and Strategies. Kluwer Academic publisher, Netherland.

Orlando, S.P., Rozas, L.P., Ward, G.H., Klein, C.J., 1993. Salinity Characteristics of Gulf of Mexico Estuaries. National Oceanic and Atmospheric Administration, Office of Ocean Resources Conservation and Assessment Silver Spring, MD 20910.

Penland, S., Ramsey, K.E., 1990. Relative Sea-Level Rise in Louisiana and the Gulf of Mexico - 1908-1988. Journal of Coastal Research 6, 323-342.

PHA, 2016. Port of Houston Authority, Overview. Available at http://www.portofhouston.com/about-us/overview/.

Pinckney, J.L., Ornolfsdottir, E.B., Lumsden, S.E., 2002. Estuarine phytoplankton group-specific responses to sublethal concentrations of the agricultural herbicide, atrazine. Mar Pollut Bull 44, 1109-1116.

Ravens, T.M., Thomas, R.C., Roberts, K.A., Santschi, P.H., 2009. Causes of Salt Marsh Erosion in Galveston Bay, Texas. Journal of Coastal Research 25, 265-272.

Ravichandran, M., Baskaran, M., Santschi, P.H., Bianchi, T.S., 1995. History of trace metal pollution in sabine-neches estuary, beaumont, Texas. Environmental Science and Technology 29, 1495-1503.

Rehkemper, L.J., 1969. Sedimentology of holocene esturine deposits, Galveston Bay. In: Holocene Geology of the Galveston Bay Area. Houston Geological Society, 12-52.

Rodriguez, A.B., Anderson, J.B., Simms, A.R., 2005. Terrace Inundation as an Autocyclic Mechanism for Parasequence Formation: Galveston Estuary, Texas, U.S.A. Journal of Sedimentary Research 75, 608-620.

Rybczyk, J.M., Cahoon, D.R., 2002. Estimating the potential for submergence for two wetlands in the Mississippi River Delta. Estuaries 25, 985-998.

Sánchez-García, L., de Andrés, J.R., Martín-Rubí, J.A., Louchouarn, P., 2009. Diagenetic state and source characterization of marine sediments from the inner continental shelf of the Gulf of Cádiz (SW Spain), constrained by terrigenous biomarkers. Organic Geochemistry 40, 184-194.

Santschi, P.H., Allison, M.A., Asbill, S., Perlet, A.B., Cappellino, S., Dobs, C., McShea, L., 1999. Sediment transport and Hg recovery in Lavaca Bay, as evaluated from radionuclide and Hg distributions. Environmental Science & Technology 33, 378-391.

Santschi, P.H., Honeyman, B.D., 1989. Radionuclides in Aquatic Environments. Radiation Physics and Chemistry 34, 213-240.

Santschi, P.H., Presley, B.J., Wade, T.L., Garcia-Romero, B., Baskaran, M., 2001. Historical contamination of PAHs, PCBs, DDTs, and heavy metals in Mississippi

River Delta, Galveston Bay and Tampa Bay sediment cores. Marine Environmental Research 52, 51-79.

Sarkanen, K.V., Ludwig, C.H., 1971. Lignins. Occurrence, Formation, Structure and Reactions. Wiley-Interscience, New York.

Shepard, F.P., 1953. Sedimentation Rates in Texas Estuaries and Lagoons. Aapg Bulletin-American Association of Petroleum Geologists 37, 1919-1934.

Shi, J.B., Ip, C.C., Zhang, G., Jiang, G.B., Li, X.D., 2010. Mercury profiles in sediments of the Pearl River Estuary and the surrounding coastal area of South China. Environ Pollut 158, 1974-1979.

Siringan, F.P., Anderson, J.B., 1993. Seismic Facies, Architecture, and Evolution of the Bolivar Roads Tidal Inlet/Delta Complex, East Texas Gulf Coast. Journal of Sedimentary Petrology 63, 794-808.

Solis, R.S., Powell, G.L., 1999. Hydrography, mixing characteristics, and residence times of Gulf of Mexico estuaries, in: Bianchi, T.S., Pennock, J.R., Twilley, R.R. (Eds.), Biogeochemistry of Gulf of Mexico Estuaries. John Wiley, New York, pp. 29-57.

Stanley, D.J., 1988. Subsidence in the northeastern nile delta: rapid rates, possible causes, and consequences. Science 240, 497-500.

Tonis, I.E., Stam, J.M.T., van de Graaf, J., 2002. Morphological changes of the Haringvliet estuary after closure in 1970. Coastal Engineering 44, 191-203.

USGS, 2002. Houston-Galveston Bay Area, Texas, From Space - A New Tool for Mapping Land Sub, USGS Fact Sheet 110-02. Available at http://pubs.usgs.gov/fs/fs-110-02/pdf/FS_110-02.pdf.

Valettesilver, N.J., 1993. The Use of Sediment Cores to Reconstruct Historical Trends in Contamination of Estuarine and Coastal Sediments. Estuaries 16, 577-588.

Ward, G.H., 1993. Dredge and fill activities in Galveston Bay, Galveston Bay National Estuary Program Publication GBNEP-28, Webster, Texas.

Wen, L.S., Santschi, P., Gill, G., Paternostro, C., 1999. Estuarine trace metal distributions in Galveston Bay: importance of colloidal forms in the speciation of the dissolved phase. Marine Chemistry 63, 185-212.

Wen, L.S., shiller, A., Santschi, P.H., Gill, G., 1999. Trace element behavior in Gulf of Mexico estuaries in: Bianchi, T.S., Pennock, J.R., Twilley, R.R. (Eds.), Biogeochemistry of Gulf of Mexico Estuaries. Wiley & Sons, Inc, Canada.

White, Tremblay, 1995. Sumbergence of wetlands as a result of human-induced subsidence and faulting along the upper Texas Gulf Coasts. Journal of Coastal Research 11, 788-807.

White, W.A., Morton, R.A., Holmes, C.W., 2002. A comparison of factors controlling sedimentation rates and wetland loss in fluvial-deltaic systems, Texas Gulf coast. Geomorphology 44, 47-66.

Williams, J., Dellapenna, T., Lee, G.-h., Louchouarn, P., 2014. Sedimentary impacts of anthropogenic alterations on the Yeongsan Estuary, South Korea. Marine Geology 357, 256-271.

Williams, J., Dellapenna, T., Louchouarn, P., Lee, G.-h., 2015. Historical reconstruction of anthropogenic mercury input from sedimentary records: Yeongsan Estuary, South Korea. Estuarine, Coastal and Shelf Science, 1-11.

Williams, J., Lee, G.-h., Shin, H.-J., Dellapenna, T., 2015. Mechanism for sediment convergence in the anthropogenically altered microtidal Nakdong Estuary, South Korea. Marine Geology 369, 79-90.

Williams, J.R., Dellapenna, T.M., Lee, G.-h., 2013. Shifts in depositional environments as a natural response to anthropogenic alterations: Nakdong Estuary, South Korea. Marine Geology 343, 47-61.

Wolanski, E., Chappell, J., 1996. The Response of Tropical Australian Estuaries to a Sea Level Rise. Journal of Marine Systems 7, 267-279.

Wu, J.H., Fu, C.Z., Chen, S.S., Chen, J.K., 2002. Soil faunal response to land use: effect of estuarine tideland reclamation on nematode communities. Applied Soil Ecology 21, 131-147.

Yeager, K.M., Brinkmeyer, R., Rakocinski, C.F., Schindler, K.J., Santschi, P.H., 2010. Impacts of Dredging Activities on the Accumulation of Dioxins in Surface Sediments of the Houston Ship Channel, Texas. Journal of Coastal Research 264, 743-752.

Yeager, K.M., Santschi, P.H., Rifai, H.S., Suarez, M.P., Brinkmeyer, R., Hung, C.-C., Schindler, K.J., Andres, M.J., Weaver, E.A., 2007. Dioxin Chronology and Fluxes in Sediments of the Houston Ship Channel, Texas: Influences of Non-Steady-State Sediment Transport and Total Organic Carbon. Environmental Science & Technology 41, 5291-5298.

Yeager, K.M., Santschi, P.H., Rowe, G.T., 2004. Sediment accumulation and radionuclide inventories (239,240Pu,210Pb and 234Th) in the northern Gulf of Mexico, as influenced by organic matter and macrofaunal density. Marine Chemistry 91, 1-14.

Yoon, H.S., Yoo, C.I., Na, W.B., Lee, I.C., Ryu, C.R., 2007. Geomorphologic evolution and mobility of sand barriers in the Nakdong estuary, South Korea. Journal of Coastal Research, 358-363.

Yuill, R.M., 1991. A Paleoecological study of a one hundred year sedimentary record of Galveston Bay, Texas, Department of Oceanography. Texas A&M Univesity, colege Station, thesis.

Zilkoski, D.B., Hall, L.W., Mitchell, G.J., Kammula, V., Singh, A., Chrismer, W.M., Neighbors, R.J., 2006. The Harris-Galveston Coastal Subsidence District/National Geodetic Survey Automated Global Positioning System Subsidence Monitoring Project. Available at http://hgsubsidence.org/wp-content/uploads/2014/07/GPS-Project.pdf.